

# Biogeochemical controls on ammonium accumulation in the surface layer of the Southern Ocean

Shantelle Smith<sup>1\*</sup>, Katye E. Altieri<sup>1</sup>, Mhlangabezi Mdutyana<sup>1,2</sup>, David R. Walker<sup>3</sup>, Ruan G. Parrott<sup>1</sup>, Sedick Gallie<sup>3</sup>, Kurt A.M. Spence<sup>1</sup>, Jessica M. Burger<sup>1</sup>, Sarah E. Fawcett<sup>1,4</sup>

<sup>1</sup> Department of Oceanography, University of Cape Town, Private Bag X3, Rondebosch, Cape Town, South Africa

<sup>2</sup> Southern Ocean Carbon and Climate Observatory (SOCCO), CSIR, Rosebank, Cape Town, South Africa

<sup>3</sup> Department of Conservation and Marine Sciences, Cape Peninsula University of Technology, Cape Town, South Africa

<sup>4</sup> Marine and Antarctic Research centre for Innovation and Sustainability (MARIS), University of Cape Town, Cape Town, South Africa

\* Corresponding author: [smtsha023@myuct.ac.za](mailto:smtsha023@myuct.ac.za)

## 1. Abstract

The production and removal of ammonium ( $\text{NH}_4^+$ ) are essential upper-ocean nitrogen cycle pathways, yet in the Southern Ocean where  $\text{NH}_4^+$  has been observed to accumulate in surface waters, its mixed-layer cycling remains poorly understood. For surface seawater samples collected between Cape Town and the marginal ice zone in winter 2017, we found that  $\text{NH}_4^+$  concentrations were five-fold higher than is typical for summer, and lower north than south of the Subantarctic Front ( $0.01\text{--}0.26\text{ }\mu\text{M}$  versus  $0.19\text{--}0.70\text{ }\mu\text{M}$ ). Our observations confirm that  $\text{NH}_4^+$  accumulates in the Southern Ocean's winter mixed layer, particularly in polar waters.  $\text{NH}_4^+$  assimilation rates were highest near the Polar Front ( $12.9 \pm 0.4\text{ nM day}^{-1}$ ) and in the Subantarctic Zone ( $10.0 \pm 1.5\text{ nM day}^{-1}$ ), decreasing towards the marginal ice zone ( $3.0 \pm 0.8\text{ nM day}^{-1}$ ) despite the high ambient  $\text{NH}_4^+$  concentrations in these southernmost waters, likely due to the low temperatures and limited light availability. By contrast, rates of  $\text{NH}_4^+$  oxidation were higher south than north of the Polar Front ( $16.0 \pm 0.8$  versus  $11.1 \pm 0.5\text{ nM day}^{-1}$ ), perhaps due to the lower light and higher iron conditions characteristic of polar waters.  $\text{NH}_4^+$  concentrations were also measured on five transects of the Southern Ocean (Subtropical- to marginal ice zone) spanning the 2018/2019 annual cycle. These measurements reveal that mixed-layer  $\text{NH}_4^+$  accumulation south of the Subantarctic Front derives from sustained heterotrophic  $\text{NH}_4^+$  production in late summer through winter that in net, outpaces  $\text{NH}_4^+$  removal by temperature-, light-, and iron-limited microorganisms. Our observations thus imply that the Southern Ocean becomes a biological source of  $\text{CO}_2$  to the atmosphere ~~in autumn and winter~~ not only because nitrate drawdown is weak, but also because the ambient conditions favour net heterotrophy and  $\text{NH}_4^+$  accumulation.

Deleted: for half the year

## 2. Introduction

The Southern Ocean impacts the Earth system through its role in global thermohaline circulation, which drives the exchange of heat and nutrients among ocean basins (Frölicher et al., 2015;

43 Sarmiento et al., 2004). The Southern Ocean also plays an integral role in mediating climate, by  
44 transferring carbon to the deep ocean via its biological and solubility pumps (Sarmiento & Orr,  
45 1991; Volk & Hoffert, 1985) and through the release of deep-ocean CO<sub>2</sub> to the atmosphere during  
46 deep-water ventilation (i.e., CO<sub>2</sub> leak; Broecker & Peng, 1992; Lauderdale et al., 2013; Sarmiento  
47 & Toggweiler, 1984). Upper Southern Ocean circulation is dominated by the eastward-flowing  
48 Antarctic Circumpolar Current (ACC) that consists of a series of broad circumpolar bands  
49 (“zones”) separated by oceanic fronts. These fronts can drive water mass formation (Ito et al.,  
50 2010) and nutrient upwelling that supports elevated productivity (Sokolov & Rintoul, 2007).

51 Concentrations of the essential macronutrients, nitrate (NO<sub>3</sub><sup>-</sup>) and phosphate (PO<sub>4</sub><sup>3-</sup>), are  
52 perennially high in Southern Ocean surface waters, in contrast to most of the global ocean.  
53 Assimilation of these nutrients, and thus primary productivity, is limited in the Southern Ocean  
54 by numerous overlapping factors, including temperature, light, micronutrient concentrations, and  
55 grazing pressure (e.g., Boyd et al., 2001; Martin et al., 1990; Reay et al., 2001; Smith Jr &  
56 Lancelot, 2004). The strength of these limitations varies with sector (i.e., longitude), zone (i.e.,  
57 latitude), and season, resulting in spatial and temporal variability in chlorophyll-a, primary  
58 production, plankton community composition, and nutrient uptake regime (Mdutyana et al.,  
59 2020; Mengesha et al., 1998; Shadwick et al., 2015; Thomalla et al., 2011). In addition to the  
60 seasonality of temperature and light, Southern Ocean ecosystems are influenced by seasonal  
61 changes in nutrient availability. In winter, deep mixing replenishes the nutrients required for  
62 phytoplankton growth but the low temperatures and light levels impede biological activity  
63 (Rintoul & Trull, 2001). Once the mixed layer shoals in spring and summer, phytoplankton  
64 consume the available nutrients until some form of limitation (usually iron; Nelson et al., 2001;  
65 Nicholson et al., 2019) sets in. This balance between wintertime nutrient recharge and  
66 summertime nutrient drawdown is central to the Southern Ocean’s role in setting atmospheric  
67 CO<sub>2</sub> (Sarmiento & Toggweiler, 1984).

68 The onset of iron limitation following the spring/early summer bloom in the Southern Ocean  
69 drives phytoplankton to increased reliance on recycled ammonium (NH<sub>4</sub><sup>+</sup>; Timmermans et al.,  
70 1998), the assimilation of which has a far lower iron requirement than that of NO<sub>3</sub><sup>-</sup> (Price et al.,  
71 1994). The extent to which phytoplankton rely on NO<sub>3</sub><sup>-</sup> versus NH<sub>4</sub><sup>+</sup> as their primary N source  
72 has implications for Southern Ocean CO<sub>2</sub> removal since phytoplankton growth fuelled by  
73 subsurface NO<sub>3</sub><sup>-</sup> (“new production”) must be balanced on an annual basis by the export of sinking  
74 organic matter (“export production”; Dugdale & Goering, 1967), which drives CO<sub>2</sub> sequestration  
75 (i.e., the biological pump; Volk & Hoffert, 1985). By contrast, phytoplankton growth on NH<sub>4</sub><sup>+</sup> or  
76 other recycled N forms (“regenerated production”) yields no net removal of CO<sub>2</sub> to the deep  
77 ocean (Dugdale & Goering, 1967). Considerable research has focused on NO<sub>3</sub><sup>-</sup> cycling in the  
78 Southern Ocean mixed layer because of the importance of this nutrient for the biological pump  
79 (e.g., Francois et al., 1992; Johnson et al., 2017; Mdutyana et al., 2020; Primeau et al., 2013;  
80 Sarmiento & Toggweiler, 1984) and global ocean fertility (Fripiat et al., 2021; Sarmiento et al.,  
81 2004). By contrast, the cycling of regenerated N within the seasonally-varying mixed layer –  
82 including the production of NH<sub>4</sub><sup>+</sup> and its removal by phytoplankton and nitrifiers – remains  
83 poorly understood.

84 NH<sub>4</sub><sup>+</sup> is produced in the euphotic zone as a by-product of heterotrophic metabolism (Herbert,  
85 1999) and as a consequence of zooplankton grazing (Lehette et al., 2012; Steinberg & Saba,

Deleted: in the Southern Ocean

2008), and is removed by phytoplankton uptake (in euphotic waters) and nitrification (mainly in aphotic waters). Heterotrophic bacteria can also consume  $\text{NH}_4^+$  (Kirchman, 1994) and have been hypothesized to do so at significant rates in the Southern Ocean mixed layer in winter (Cochlan, 2008; Mduyana et al., 2020). The assimilation of  $\text{NH}_4^+$  by phytoplankton requires relatively little energy (Dortch, 1990) such that  $\text{NH}_4^+$  is usually consumed in the euphotic zone as rapidly as it is produced (Glibert, 1982; La Roche, 1983), resulting in very low surface  $\text{NH}_4^+$  concentrations in the open ocean ( $<0.2 \mu\text{M}$ ; Paulot et al., 2015). Additionally,  $\text{NH}_4^+$  is often the preferred N source to small phytoplankton (Dortch 1990), which typically dominate when iron and/or light are limiting (Deppeler & Davidson, 2017; Pearce et al., 2010; Tagliabue et al., 2014) since their higher cell surface area-to-volume ratio renders them less vulnerable to diffusion- and/or light limitation (Finkel et al., 2004; Fujiki & Taguchi, 2002; Hudson & Morel, 1993; Mei et al., 2009).

In addition to the implications for size distribution, the dominant N source to phytoplankton is indicative of their potential for  $\text{CO}_2$  removal, as per the new production paradigm (Dugdale & Goering, 1967). The N isotopic composition ( $\delta^{15}\text{N}$ , in ‰ vs.  $\text{N}_2$  in air,  $= (^{15}\text{N}/^{14}\text{N}_{\text{sample}}/^{15}\text{N}/^{14}\text{N}_{\text{air}} - 1) \times 1000$ ) of particulate organic N (PON; a proxy for phytoplankton biomass) can be used to infer the dominant N source to phytoplankton (Altabet, 1988; Fawcett et al., 2011; 2014; Lourey et al., 2003; Van Oostende et al., 2017) since the assimilation of subsurface  $\text{NO}_3^-$  yields PON that is higher in  $\delta^{15}\text{N}$  than that fuelled by recycled  $\text{NH}_4^+$  uptake (Treibergs et al., 2014). As such, measurements of bulk  $\delta^{15}\text{N}$ -PON can be used to infer the net N uptake regime,

Deleted: (Altabet, 1988; Fawcett et al., 2011; 2014; Lourey et al., 2003)

Nitrification, the oxidation of  $\text{NH}_4^+$  to nitrite ( $\text{NO}_2^-$ ) and then  $\text{NO}_3^-$  by chemoautotrophic bacteria and archaea, was historically considered unimportant in euphotic zone waters due to the evidence for light inhibition of nitrifiers (Hooper & Terry, 1974; Horrigan & Springer, 1990; Olson, 1981) and the fact that they are outcompeted by phytoplankton for  $\text{NH}_4^+$  (Smith et al., 2014; Ward, 1985; 2005; Zakem et al., 2018). However, this view has been challenged in numerous ocean regions (Yool et al., 2007), including the Southern Ocean (Smart et al., 2015; Cavagna et al., 2015; Fripiat et al., 2015; Mduyana et al., 2020). Wintertime upper-ocean  $\text{NH}_4^+$  dynamics thus have implications for annual estimates of carbon export potential, insofar as  $\text{NO}_3^-$  produced by nitrification in the winter mixed layer that is subsequently supplied to spring and summer phytoplankton communities constitutes a regenerated rather than a new N source on an annual basis (Mduyana et al., 2020).

Deleted: /

Surface concentrations of  $\text{NH}_4^+$  are typically near-zero in spring and early- to mid-summer in the open Southern Ocean (Daly et al., 2001; Henley et al., 2020; Sambrotto & Mace, 2000; Savoye et al., 2004) due to assimilation by phytoplankton. In late summer, a peak in  $\text{NH}_4^+$  concentration has been observed and attributed to enhanced bacterial and zooplankton activity following elevated phytoplankton growth (Becquevort et al., 2000; Dennett et al., 2001; Mengesha et al., 1998). The limited available observations suggest that wintertime surface  $\text{NH}_4^+$  concentrations are high (often  $>1 \mu\text{M}$ ), particularly south of the Subantarctic Front (SAF) (Bianchi et al., 1997; Henley et al., 2020; Philibert et al., 2015; Mduyana et al., 2020; Weir et al., 2020). It thus appears that  $\text{NH}_4^+$  is not depleted following the late summer peak in its concentration, which indicates enhanced  $\text{NH}_4^+$  regeneration, either coincident with (but in excess of)  $\text{NH}_4^+$  assimilation in winter and/or prior to this in late summer and/or autumn. Under these conditions, the Southern Ocean mixed layer may become net heterotrophic and thus a biological source of  $\text{CO}_2$  to the atmosphere.

Here, we focus on  $\text{NH}_4^+$  cycling in the Southern Ocean mixed layer, mainly in winter, which is a season assumed to be largely biologically dormant (Arrigo et al., 2008; Schaafsma et al., 2018) and for which  $\text{NH}_4^+$  cycle data are scarce. We confirm that  $\text{NH}_4^+$  accumulates throughout the winter mixed layer south of the SAF, and examine the potential drivers thereof. Using  $\text{NH}_4^+$  concentration data collected over a full annual cycle, we propose that these drivers include a contribution from the residual late-summer  $\text{NH}_4^+$  pool, sustained  $\text{NH}_4^+$  production in the autumn and winter, and limited wintertime  $\text{NH}_4^+$  uptake and oxidation that nonetheless exceed the rate of in situ  $\text{NH}_4^+$  production. Finally, from our temporally-resolved  $\text{NH}_4^+$  concentration data, we propose – for the first time – a measurement-based seasonal cycle for the mixed-layer  $\text{NH}_4^+$  pool south of the SAF.

### 3. Methods

#### 3.1 Cruise tracks and sample collection

Samples were collected for a series of analyses on the southward (S) and northward (N) legs of a winter cruise between Cape Town, South Africa, and the marginal ice zone (MIZ) onboard the R/V *SA Agulhas II* (VOY025; 28 June to 13 July 2017) (Fig. 1). Samples were also collected for  $\text{NH}_4^+$  concentration analysis on three cruises onboard the R/V *SA Agulhas II* during 2018/19: early- and late summer samples were collected during the SANAE 58 Relief Voyage (6 December 2018 to 15 March 2019; VOY035); winter samples were collected during the SCALE 2019 (www.scale.org.za) winter cruise to the MIZ (18 July to 12 August 2019; VOY039); and spring samples were collected during the SCALE 2019 spring cruise to the MIZ (12 October to 20 November 2019; VOY040) (Fig. S1).

Leg S of VOY025 in winter 2017 crossed the Atlantic sector and due to logistical constraints, involved only surface underway collections, while leg N bordered the Atlantic and Indian sectors (30°E; WOCE IO6 line) and included eight conductivity-temperature-depth (CTD) hydrocast stations. Frontal positions were determined using the ship's hull-mounted thermosalinograph, supported by temperature, salinity, and oxygen concentration data from CTD measurements made during leg N. The salinity and oxygen sensors were calibrated against seawater samples that were analyzed for salinity using a Portasal 8410A salinometer and for dissolved oxygen by Winkler titration (Strickland & Parsons, 1972). Frontal positions were determined from sharp gradients in potential temperature, salinity, potential density, and oxygen concentrations (Belkin & Gordon, 1996; Lutjeharms & Valentine, 1984; Orsi et al., 1995). For leg N, the mixed layer depth (MLD) was determined for each Niskin (up)cast as the depth between 10 m and 400 m at which the Brunt Väisälä Frequency squared,  $N^2$ , reached a maximum (Carvalho et al., 2017).

During leg S, samples were collected every four hours from the ship's underway system (~7 m intake; "underway stations") while samples on leg N were collected from surface Niskin bottles (~10 m, approximately 55% light depth) mounted on the CTD rosette ("CTD stations").  $\text{NH}_4^+$  samples were also taken at 13 depths over the upper 500 m at the CTD stations. During the 2018/19 cruises,  $\text{NH}_4^+$  samples were collected every two hours from the ship's underway system. At all stations, 40 mL of unfiltered seawater was collected for the analysis of  $\text{NH}_4^+$  concentrations in duplicate 50 mL high density polyethylene (HDPE) bottles that had been stored ("aged") with orthophthaldialdehyde (OPA) working reagent. Unfiltered seawater was collected in duplicate

Deleted: mainly

175 50 mL polypropylene centrifuge tubes for the analysis of  $\text{NO}_3^-$ ,  $\text{NO}_2^-$ , and  $\text{PO}_4^{3-}$ , and in a single  
176 tube for urea. Immediately following collection,  $\text{NH}_4^+$  and nutrient samples were frozen at  $-20^\circ\text{C}$ .

177 Duplicate size-fractionated chlorophyll-a samples were collected by filtering seawater (500 mL)  
178 through 25 mm-diameter glass fibre filters (0.3  $\mu\text{m}$  and 2.7  $\mu\text{m}$ ; Sterlitech GF-75 and Grade D,  
179 respectively). Acetone (90%) was added to foil-wrapped borosilicate tubes containing the filters  
180 and incubated at  $-20^\circ\text{C}$  for 24 hours. Duplicate seawater samples (4 L) were also gently vacuum-  
181 filtered through combusted 47 mm-diameter, 0.3  $\mu\text{m}$  GF-75 and 2.7  $\mu\text{m}$  Grade-D filters for POC  
182 and PON concentrations and  $\delta^{15}\text{N}$ -PON. Filters were stored in combusted foil envelopes at  
183  $-80^\circ\text{C}$ .

184 For microscopy, unfiltered seawater samples (250 mL) were collected during leg S in amber  
185 glass bottles and immediately fixed by the addition of 2.5 mL of Lugol's iodine solution (2%  
186 final concentration), then stored at low room temperature in the dark until analysis. For flow  
187 cytometry, seawater samples were collected in triplicate 2 mL microcentrifuge tubes, fixed with  
188 glutaraldehyde (1% final concentration), and stored at  $-80^\circ\text{C}$  until analysis (Marie et al., 2005).

189 Ten incubation experiments were conducted during leg S to measure net primary production  
190 (NPP). In addition, four NPP experiments were conducted during leg N using seawater collected  
191 from Niskin bottles fired at  $\sim 10$  m. In all cases, pre-screened (200- $\mu\text{m}$  mesh; to remove large  
192 grazers) seawater was collected in three 2-L polycarbonate bottles to which  $\text{NaH}^{13}\text{CO}_3$  was added  
193 at  $\sim 5\%$  of the estimated ambient DIC concentration.  $^{13}\text{C}$  enrichment was re-calculated post-cruise  
194 using measured DIC concentrations, and these enrichments were used in all NPP rate  
195 calculations. Bottles were incubated for 5 to 6.5 hours in custom-built deck-board incubators  
196 shaded with neutral-density screens to mimic the 55% light level and supplied with running  
197 surface seawater. Following incubation, each sample was divided (1 L per size fraction) and  
198 gently vacuum filtered through combusted 0.3  $\mu\text{m}$  and 2.7  $\mu\text{m}$  glass fibre filters that were stored  
199 in combusted foil at  $-80^\circ\text{C}$  until analysis.

200 N uptake (as  $\text{NO}_3^-$ ,  $\text{NH}_4^+$  and urea) and  $\text{NH}_4^+$  oxidation experiments were conducted at five  
201 stations during leg S, with  $\text{NH}_4^+$  oxidation measured at two additional stations at the ice edge  
202 (Fig. 1). On leg N, experiments were also conducted using seawater collected from  $\sim 10$  m at the  
203 same four CTD stations as the NPP experiments. Duplicate 1 L polycarbonate bottles were  
204 amended with  $^{15}\text{N}$ -labeled  $\text{NO}_3^-$ ,  $\text{NH}_4^+$  or urea at  $\sim 10\%$  of the ambient N concentration, estimated  
205 based on past wintertime measurements (Mdutyana et al., 2020) and, in the case of  $\text{NH}_4^+$ ,  
206 coincident shipboard analyses.  $^{15}\text{N}$  enrichment was re-calculated post-cruise using the measured  
207 nutrient concentrations, and these enrichments were used in all rate calculations. Incubations and  
208 filtration were carried out as for NPP, although 500 mL was used per size fraction. For  $\text{NH}_4^+$   
209 oxidation, duplicate black 250 mL HDPE bottles were amended with 0.1  $\mu\text{M}$   $^{15}\text{NH}_4^+$  and 0.1  $\mu\text{M}$   
210  $^{14}\text{NO}_2^-$  (the latter as a "trap" for the  $^{15}\text{NO}_2^-$  produced by  $\text{NH}_4^+$  oxidation; Ward 2011).  $\text{NH}_4^+$   
211 oxidation bottles were incubated for 24 hours under the same temperature conditions as the N  
212 uptake and NPP experiments. Subsamples (50 mL) were collected from each bottle immediately  
213 following tracer addition ( $T_0$ ) and at the end of the experiments ( $T_f$ ), and frozen at  $-20^\circ\text{C}$  until  
214 analysis.

### 215 3.2 Sample processing

216 3.2.1. Ammonium concentrations

217 On all cruises,  $\text{NH}_4^+$  concentrations were measured shipboard using the fluorometric method of  
218 Holmes et al. (1999) and a Turner Designs Trilogy fluorometer 7500-000 equipped with a UV  
219 module. The detection limit, calculated as twice the pooled standard deviation of all standards,  
220 was  $0.06 \mu\text{M}$ . To prevent possible in/efflux of ammonia ( $\text{NH}_3$ ) due to the temperature difference  
221 between surface waters and the shipboard laboratory, samples were frozen immediately upon  
222 collection, for a maximum of 24 hours. OPA working reagent was added to the frozen samples  
223 prior to defrosting them for analysis. Samples were slowly warmed to room temperature in a  
224 water bath after OPA addition, incubated in the dark for four hours once defrosted, and then each  
225 replicate was measured in triplicate. Standards and blanks were made daily using Type-1 Milli-  
226 Q water. Precision was  $\pm 0.03 \mu\text{M}$  for replicate samples and standards.

227 During VOY040 (spring 2019), we investigated the possibility that the ship's underway system  
228 alters the seawater  $\text{NH}_4^+$  concentrations (e.g., due to contamination or cell breakage). We  
229 collected surface samples from the underway and Niskin bottles concurrently and measured an  
230 average  $\text{NH}_4^+$  concentration difference of  $0.07 \pm 0.15 \mu\text{M}$  ( $n=17$ ), with no noticeable trend of  
231 one method consistently yielding higher/lower concentrations. We thus have no reason to doubt  
232  $\text{NH}_4^+$  concentrations measured for seawater samples collected from the ship's underway system.

233 3.2.2. Macronutrient concentrations

234 Following the winter 2017 cruise, duplicate seawater samples were analysed manually for  $\text{NO}_2^-$   
235 and  $\text{PO}_4^{3-}$  (Bendschneider & Robinson, 1952; Murphy & Riley, 1962) using a Thermo Scientific  
236 Genesys 30 Visible spectrophotometer. Precision and detection limit was  $\pm 0.05 \mu\text{M}$  and  $0.05$   
237  $\mu\text{M}$  for  $\text{NO}_2^-$  and  $\pm 0.06 \mu\text{M}$  and  $0.05 \mu\text{M}$  for  $\text{PO}_4^{3-}$ . The concentrations of  $\text{NO}_3^- + \text{NO}_2^-$  and  
238  $\text{Si}(\text{OH})_4$  were measured using a Lachat QuickChem 8500 Series 2 flow injection autoanalyzer.  
239 Aliquots of a certified reference material (JAMSTEC) were measured during each run to ensure  
240 measurement accuracy ( $\text{SD} \leq 2\%$ ). The precision of the  $\text{NO}_3^- + \text{NO}_2^-$  and  $\text{Si}(\text{OH})_4$  measurements  
241 was  $\pm 0.4 \mu\text{M}$  and  $\pm 0.2 \mu\text{M}$ , respectively, and the detection limit was  $0.1 \mu\text{M}$  and  $0.2 \mu\text{M}$ .  $\text{NO}_3^-$   
242 concentrations were calculated by subtraction (i.e.,  $\text{NO}_3^- + \text{NO}_2^- - \text{NO}_2^-$ ), with error propagated  
243 according to standard statistical practices. Urea-N (hereafter, urea) concentrations were  
244 determined via the room-temperature, single-reagent colorimetric method (Revilla et al., 2005)  
245 using a Thermo Scientific Genesys 30 Visible spectrophotometer; precision was  $\pm 0.04 \mu\text{M}$  and  
246 the detection limit was  $0.04 \mu\text{M}$ .

247 3.2.3. Chlorophyll-a concentrations

248 Chlorophyll-a concentrations ([chl-a]) were determined shipboard using the nonacidified  
249 fluorometric method (Welschmeyer, 1994). The Turner Designs Trilogy fluorometer was  
250 calibrated with an analytical standard (*Anacystis nidulans*, Sigma-Aldrich®) prior to and  
251 following the cruise. The [chl-a] of the  $0.3\text{-}2.7 \mu\text{m}$  size class (hereafter, "pico" size class) was  
252 calculated by subtracting the measured [chl-a] of the  $>2.7 \mu\text{m}$  size class (hereafter, "nano+" size  
253 class) from the  $>0.3 \mu\text{m}$  size class (hereafter, "bulk"). Given previous work showing that the  
254 winter Southern Ocean phytoplankton community is composed primarily of small cells (i.e.,  
255 typically  $<15 \mu\text{m}$ ; e.g., Hewes et al., 1985; 1990; Weber & El-Sayed, 1987), we did not separate  
256 micro- from nanophytoplankton.

#### 3.2.4. Bulk POC, PON and $\delta^{15}\text{N}$ -PON

The NPP and N uptake filters were fumed with hydrochloric acid in a desiccator for 24 hours to remove inorganic carbon, then dried for 24 hours at 40°C and packaged into tin cups. Filters for  $\delta^{15}\text{N}$ -PON were dried in the same way, but not acidified. Samples were analysed using a Delta V Plus isotope ratio mass spectrometer (IRMS) coupled to a Flash 260 elemental analyser, with a detection limit of 0.17  $\mu\text{mol C}$  and 0.07  $\mu\text{mol N}$  and precision of  $\pm 0.005 \text{ At\%}$  for C and N. Unused pre-combusted filters (blanks) were included in each batch run. POC and PON content was determined from daily standard curves of IRMS area versus known C and N masses. For the isotope ratios, sample measurements were referenced to internal laboratory standards calibrated against IAEA reference materials that were measured after every 5-7 samples.

#### 3.2.5. Size-fractionated rates of NPP and N uptake

Carbon and N uptake rates (NPP,  $\rho\text{NH}_4^+$ ,  $\rho\text{NO}_3^-$ ,  $\rho\text{Urea}$ ) were calculated according to Dugdale & Wilkerson (1986) as:

$$\rho M = \frac{[PM] \times (At\%_{meas} - At\%_{amb})}{T \times (At\%_{init} - At\%_{amb})} \quad (\text{Eqn 1})$$

$$\text{where, } At\%_{init} = \frac{([M] \times At\%_{amb}) + ([M_{tracer}] \times At\%_{tracer})}{[M] + [M_{tracer}]} \quad (\text{Eqn 2})$$

Here, M is the species of interest (C,  $\text{NH}_4^+$ ,  $\text{NO}_3^-$ , or urea);  $\rho M$  is the uptake rate of that species ( $\text{nM hour}^{-1}$ , i.e.,  $\text{nmol C or N L}^{-1} \text{ hour}^{-1}$ ); [PM] is the concentration of POC or PON ( $\mu\text{M}$ ) on the filters; [M] is the ambient concentration of DIC,  $\text{NH}_4^+$ ,  $\text{NO}_3^-$ , or urea at the time of sample collection;  $[M_{tracer}]$  is the concentration of  $\text{NaH}^{13}\text{CO}_3$ ,  $^{15}\text{NH}_4^+$ ,  $^{15}\text{NO}_3^-$ , or  $^{15}\text{N}$ -urea added to the incubation bottles; and T is the incubation period (days). DIC concentrations were measured shipboard using a VINDTA 3C instrument and ranged from 2017 to 2130  $\mu\text{M}$  (Bakker et al., 2016). The PM and  $\rho M$  of the picoplankton size class was calculated by subtracting the nanoplankton from the bulk measurements. Daily rates were computed by multiplying the hourly rates by the number of daylight hours, the latter calculated using the sampling latitude and day of the year (Forsythe et al., 1995).

The f-ratio (Eppley & Peterson, 1979), used to estimate the fraction of NPP potentially available for export, was calculated as:

$$f - \text{ratio} = \frac{\rho\text{NO}_3^-}{\rho N_{tot}} \quad (\text{Eqn 3})$$

where  $\rho N_{tot} = \rho\text{NH}_4^+ + \rho\text{NO}_3^- + \rho\text{Urea}$ . Urea uptake was not measured at underway stations 50.7°S and 55.5°S (both in the Antarctic Zone); here, the f-ratio was calculated omitting  $\rho\text{Urea}$ . For the two Antarctic Zone stations at which urea uptake was measured, including  $\rho\text{Urea}$  decreased the f-ratio by 8-25% compared to that calculated using only  $\rho\text{NO}_3^-$  and  $\rho\text{NH}_4^+$ .

#### 3.2.6. Ammonia oxidation rates

The azide method (McIlvin and Altabet 2005) was used to convert  $\text{NO}_2^-$  produced by  $\text{NH}_4^+$  oxidation to  $\text{N}_2\text{O}$  gas that was measured using a Delta V Plus IRMS with a custom-built purge-

and-trap front end (McIlvin & Casciotti, 2011). This configuration yields a detection limit of 0.2 nmol N with a  $\delta^{15}\text{N}$  precision of  $\pm 0.1\%$ . The  $\delta^{15}\text{N}$  of  $\text{NO}_2^-$  was derived from  $^{45}\text{N}_2\text{O}/^{44}\text{N}_2\text{O}$  and the rate of  $\text{NH}_4^+$  oxidation ( $\text{NH}_4^+_{\text{ox}}$ ,  $\text{nM day}^{-1}$ ) was calculated following Peng et al. (2015) as:

$$\text{NH}_4^+_{\text{ox}} = \frac{\Delta[^{15}\text{NO}_2^-]}{f_{\text{NH}_4^+}^{15} \times T} \quad (\text{Eqn 4})$$

Here,  $\Delta[^{15}\text{NO}_2^-]$  is the change in the concentration of  $^{15}\text{NO}_2^-$  (nM) between the start and end of the incubation, calculated as the difference in the measured  $\delta^{15}\text{N}$  of  $\text{NO}_2^-$  between the  $T_i$  and  $T_0$  samples,  $f_{\text{NH}_4^+}^{15}$  is the fraction of the  $\text{NH}_4^+$  substrate labelled with  $^{15}\text{N}$  at the start of the incubation, and  $T$  is the incubation length (days). All  $^{15}\text{NO}_2^-$  produced during the incubations was assumed to derive from  $^{15}\text{NH}_4^+$  oxidation. The detection limit ranged from 0.02 to 0.11  $\text{nM day}^{-1}$ , calculated according to Santoro et al. (2013).

We note that isotope dilution (i.e., the dilution of  $^{15}\text{NH}_4^+$  by co-occurring  $^{14}\text{NH}_4^+$  regeneration) during the  $\text{NH}_4^+$  uptake and oxidation experiments could potentially lead to an underestimation of the rates (Glibert et al., 1982; Mdotyana, 2021). For the  $\text{NH}_4^+$  uptake experiments, their short duration (3 to 7.5 hours) would have rendered the effect of regeneration minor (Mdotyana et al., 2020). Moreover, the  $^{15}\text{NH}_4^+$  additions were high (100 nM) relative to both the ambient  $\text{NH}_4^+$  concentrations north of the SAF and the  $K_m$  values derived for  $\text{NH}_4^+$  uptake and oxidation in the winter Southern Ocean (150-405 nM and 28-137 nM, respectively; Mdotyana, 2021), making a significant dilution effect unlikely (Lipschultz, 2008). Finally, at the stations south of the SAF, the ambient  $\text{NH}_4^+$  concentrations were so high that even if the regeneration of  $^{14}\text{NH}_4^+$  occurred at an elevated rate (e.g., 50  $\text{nM day}^{-1}$ ; as has been measured in the late-summer Southern Ocean when remineralization is expected to be high; Goeyens et al., 1991), the  $^{15}\text{N}/^{14}\text{N}$  of the  $\text{NH}_4^+$  pool would decrease by <1-2%. We thus consider the potential effect of isotope dilution to be minor.

A further consideration is possible stimulation of the  $\text{NH}_4^+$  uptake and oxidation rates by  $^{15}\text{NH}_4^+$  addition (Lipschultz, 2008). Given the  $K_m$  values listed above and the high ambient  $\text{NH}_4^+$  concentrations measured in the PFZ and AZ, a stimulation effect could only be significant at the stations north of the SAF where the  $\text{NH}_4^+$  concentrations were 10-100 nM, and even then, to a lesser extent for  $\text{NH}_4^+$  oxidation than  $\text{NH}_4^+$  uptake given that ammonia oxidizers in the winter Southern Ocean become saturated at  $\text{NH}_4^+$  concentrations of 100-200 nM (Mdotyana, 2021). The rates reported for the stations north of the SAF should therefore be considered “potential rates.” However, since our focus is mainly on explaining the accumulation of  $\text{NH}_4^+$  south of the SAF, having “potential” rather than “true” rates for the STZ and SAZ does not affect our conclusions.

### 3.2.7 Plankton community composition

Microplankton groups ( $>15 \mu\text{m}$ ) were identified and counted in a subsample (20 mL) from each amber bottle using the Utermöhl technique (Utermöhl, 1958) and following the recommendations of Hasle (1978). Plankton groups and individual species were counted and identified using an inverted light microscope (Olympus CKX41) at 200x magnification. This level of magnification limited the cell sizes that could be reliably distinguished to  $>15 \mu\text{m}$ . For each sample, at least 100 cells were enumerated to ensure a statistically valid count.



Pico- and nanoplankton cells (<15 µm) were enumerated using an LSR II flow cytometer (BD Biosciences) equipped with blue, red, violet, and green lasers. Prior to analysis, 1 mL of sample was incubated with 1% (v/v) SYBR Green-I (a DNA stain) at room temperature in the dark for 10 minutes (Marie et al., 1997). From light scatter and autofluorescence, the DNA-containing particles were identified as nano- and picoeukaryotes, and *Synechococcus*. Additionally, small heterotrophic prokaryotes (i.e., bacteria and possibly archaea; hereafter “bacteria”) were identified as DNA-containing particles with the lowest detectable autofluorescence (Marie et al., 1997; Gasol & del Giorgio, 2000) (see also Text S2). All particles lacking DNA were considered detritus. The populations of interest were gated using FlowJo 10.3 software (TreeStar, Inc.; [www.flowjo.com](http://www.flowjo.com)).

In this study, we did not directly measure NH<sub>4</sub><sup>+</sup> regeneration (i.e., heterotrophy). Instead, we use the abundance of heterotrophic bacteria as a qualitative indicator of NH<sub>4</sub><sup>+</sup> regeneration potential, recognizing that cell abundance does not imply activity. Additionally, we estimate the rate of NH<sub>4</sub><sup>+</sup> production from our concentration and rate data (see section 3.3). The availability of organic matter to heterotrophs is inferred from the abundance of detritus.

### 3.3 Mixed-layer NH<sub>4</sub><sup>+</sup> residence time and NH<sub>4</sub><sup>+</sup> production rate estimates

The residence time of the mixed-layer NH<sub>4</sub><sup>+</sup> pool can be estimated using the measured ambient NH<sub>4</sub><sup>+</sup> concentrations and corresponding NH<sub>4</sub><sup>+</sup> removal rates as

$$NH_4^+ \text{ residence time} = \frac{[NH_4^+]}{NH_4^+ \text{ removal rate}} \quad (\text{Eqn 5})$$

Here, NH<sub>4</sub><sup>+</sup> residence time is the time period (days) over which a given NH<sub>4</sub><sup>+</sup> concentration will be depleted assuming a constant NH<sub>4</sub><sup>+</sup> removal rate. We set NH<sub>4</sub><sup>+</sup> removal rate = ρNH<sub>4</sub><sup>+</sup> + NH<sub>4</sub><sup>+</sup> ox in winter and = ρNH<sub>4</sub><sup>+</sup> in late summer given the evidence for negligible mixed-layer NH<sub>4</sub><sup>+</sup> oxidation rates in this latter season (Bianchi et al., 1997; Mdutyana et al., 2020).

To determine the contribution of late summer NH<sub>4</sub><sup>+</sup> production to the wintertime NH<sub>4</sub><sup>+</sup> pool (see section 5.2), we define a rate of NH<sub>4</sub><sup>+</sup> concentration decline:

$$NH_4^+ \text{ rate of decline} = NH_4^+ \text{ production rate} - NH_4^+ \text{ removal rate} \quad (\text{Eqn 6})$$

Here, NH<sub>4</sub><sup>+</sup> production rate is the NH<sub>4</sub><sup>+</sup> flux required to compensate for NH<sub>4</sub><sup>+</sup> removal over the late-summer-to-winter period, in order to yield the observed seasonal change in the ambient NH<sub>4</sub><sup>+</sup> concentration.

The rate of NH<sub>4</sub><sup>+</sup> concentration decline can also be defined as:

$$NH_4^+ \text{ rate of decline} = \frac{[NH_4^+]_{\text{decline}}}{t} \quad (\text{Eqn 7})$$

Where [NH<sub>4</sub><sup>+</sup>]<sub>decline</sub> is the difference between the late summer and winter NH<sub>4</sub><sup>+</sup> concentrations and *t* is the time period (days) over which the NH<sub>4</sub><sup>+</sup> concentration declines. Setting Eqn 6 and 7 equal yields:

$$NH_4^+ \text{ production rate} = \frac{[NH_4^+]_{\text{decline}}}{t} + NH_4^+ \text{ removal rate} \quad (\text{Eqn 8})$$

Where,  $\text{NH}_4^+ \text{ removal rate} = \rho \text{NH}_4^+ + \text{NH}_4^+ \text{ ox}$ . Eqns 7 and 8 assume that the elevated wintertime  $\text{NH}_4^+$  concentrations result from continuous  $\text{NH}_4^+$  production in excess of removal rather than from sporadic events of removal and/or production occurring between late summer and winter.

Deleted: consumption

### 3.4 Statistical analyses

The correlations among latitude, N concentrations, NPP, N assimilation rates, and  $\text{NH}_4^+$  oxidation rates were investigated at the 5% significance level using the Pearson correlation coefficient and the R packages, stats (R Core Team, 2020) and corrplot (Wei & Simko, 2017). Standard deviations were propagated using standard statistical practices.

## 4. Results

### 4.1 Hydrography

Sea surface temperature (SST) decreased by  $\sim 17^\circ\text{C}$  between Cape Town ( $\sim 34^\circ\text{S}$ ) and the edge of the MIZ ( $61.7^\circ\text{S}$ ), with similar gradients measured for legs S and N. During leg N, fairly deep MLDs were observed (124–212 m), similar to June and July climatological MLDs compiled from Argo float data for this region (Dong et al., 2008). While the focus of this study is the surface (i.e., upper  $\sim 10$  m), we report the MLDs here to show that sampling took place under typical winter conditions, with the deep MLDs evincing ongoing winter mixing and associated nutrient recharge. Where not specified, the trends discussed below refer to the surface data only. Latitudinal variations in each parameter are assessed by comparing the various Southern Ocean zones – the Subtropical Zone (STZ) north of the Subtropical Front (STF), the Subantarctic Zone (SAZ) between the STF and the Subantarctic Front (SAF), the Polar Frontal Zone (PFZ) between the SAF and the Polar Front (PF), and south of the PF, the Open and Polar Antarctic Zones (OAZ and PAZ, which are divided by the Southern Antarctic Circumpolar Current Front (SACCF) and collectively termed the Antarctic Zone (AZ); see Text S1 for detailed definitions of the fronts and zones, and Fig. 1 and S1 for their positions at the time of sampling). For each parameter, the average  $\pm 1$  standard deviation (SD) for each Southern Ocean zone is reported in Table 1.

### 4.2 Macronutrient concentrations

In winter 2017, the surface and mixed-layer concentrations of  $\text{NH}_4^+$  ranged from below detection to  $0.70\ \mu\text{M}$  (Fig. 2a and b). Surface concentrations were higher in the PFZ, OAZ, and PAZ ( $0.42 \pm 0.01\ \mu\text{M}$ ,  $0.52 \pm 0.01\ \mu\text{M}$ , and  $0.58 \pm 0.01\ \mu\text{M}$ , respectively) than in the STZ and SAZ ( $0.08 \pm 0.03\ \mu\text{M}$  and  $0.06 \pm 0.01\ \mu\text{M}$ , respectively), with a sharp gradient observed at the SAF. South of the SAF, high  $\text{NH}_4^+$  concentrations persisted near-homogeneously throughout the mixed layer, with mixed layer averages ranging from  $0.65 \pm 0.01\ \mu\text{M}$  at station  $58.5^\circ\text{S}$  to  $0.27 \pm 0.01\ \mu\text{M}$  at station  $48.0^\circ\text{S}$  and averaging  $0.47 \pm 0.02\ \mu\text{M}$ , with concentrations that were below detection north of the SAF (Fig. 2b). Below the mixed layer,  $\text{NH}_4^+$  concentrations decreased rapidly at all stations to values below detection by 200 m.

The concentrations of  $\text{NO}_3^-$  and  $\text{PO}_4^{3-}$  increased southwards from  $<10\ \mu\text{M}$  and  $<1\ \mu\text{M}$  in the STZ to  $>20\ \mu\text{M}$  and  $>1.5\ \mu\text{M}$  in the PFZ, OAZ, and PAZ (Fig. 2c and S3a), with the sharpest gradients occurring near the SAF. The concentrations of  $\text{Si(OH)}_4$  increased rapidly across the PF, from an average of  $3.2 \pm 1.1\ \mu\text{M}$  between  $35.0^\circ\text{S}$  and  $48.0^\circ\text{S}$  to  $45.6 \pm 0.6\ \mu\text{M}$  between  $52.1^\circ\text{S}$  and  $58.9^\circ\text{S}$

(Fig. S3b). The  $\text{NO}_2^-$  concentrations were consistently low across the transect ( $0.16 \pm 0.02 \mu\text{M}$ ; Fig. S3c), as were the concentrations of urea ( $0.20 \pm 0.04 \mu\text{M}$ ; Table 1), with slightly lower urea concentrations observed in the SAZ than in the other zones.

#### 4.3 Chlorophyll-a, POC and PON

The highest bulk [chl-a] was observed near the South African continental shelf, decreasing across the STF and remaining low thereafter (Fig. 3a). The proportion of chl-a in the nano+ size class varied across the region but was  $>50\%$  at all stations, with higher ( $>80\%$ ) contributions near the fronts and at many OAZ and PAZ stations (Fig. 3b). The nano+ contribution was  $\leq 60\%$  at only five stations (three in the SAZ, two in the OAZ).

The concentrations of bulk POC and PON were highest north of the STF and slightly higher in the OAZ than in the SAZ and PFZ (Fig. S4a and b). The contribution of the nano+ size fraction to POC and PON across the transect was  $77.1 \pm 22.6\%$  and  $66.9 \pm 24.2\%$ , respectively (Fig. S4c and d). The  $\delta^{15}\text{N}$ -PON decreased southwards from the STZ and SAZ ( $1.7 \pm 1.0\text{‰}$ ) to the PFZ and OAZ ( $0.5 \pm 0.5\text{‰}$ ; Fig. 4). Despite considerable differences among zones, the  $\delta^{15}\text{N}$ -PON was relatively homogenous within each zone.

#### 4.4 Rates of net primary production, nitrogen uptake, and ammonium oxidation

Rates of bulk NPP were two- to six-fold higher in the SAZ and PFZ than has been reported previously for the Atlantic sector in winter (Mdutyana et al., 2020; Froneman et al., 1999) (Fig. 5a). By contrast, NPP was low in the OAZ, consistent with previous measurements (Kottmeier & Sullivan, 1987; Mdutyana et al., 2020). The relative contribution of the nano+ size class generally decreased southwards, from 85.4% at 37.0°S to 24.4% at 53.5°S, before increasing to  $>80\%$  near the SACCF.

The bulk  $\text{NH}_4^+$  uptake rates ( $\rho\text{NH}_4^+$ ) generally increased southwards from the STZ to the SAZ and PFZ, and then decreased across the OAZ to reach a minimum at the southernmost station (Fig. 5b). In the nano+ size fraction,  $\rho\text{NH}_4^+$  changed little latitudinally, although it was slightly lower in the PFZ than in the other zones. The contribution of nanoplankton to  $\rho\text{NH}_4^+$  ranged from 32.8% in the PFZ to 71.9% in the STZ. The bulk  $\text{NO}_3^-$  uptake rates ( $\rho\text{NO}_3^-$ ) were also low in the STZ, while the highest  $\rho\text{NO}_3^-$  was measured in the SAZ, with the rate then decreasing southwards.  $\rho\text{NO}_3^-$  in the nano+ size class followed the same trend as total community  $\rho\text{NO}_3^-$ , with the nanoplankton accounting for  $71.5 \pm 0.3\%$  of bulk  $\rho\text{NO}_3^-$  on average. The rates of bulk urea uptake ( $\rho\text{Urea}$ ) were highest in the STZ, with the SAZ and the PFZ hosting similar rates, and the lowest rates were measured in the OAZ.  $\rho\text{Urea}$  for the nano+ size class followed a similar trend to bulk  $\rho\text{Urea}$ , and nanoplankton accounted for 51.8% of  $\rho\text{Urea}$  in the SAZ, increasing to 100% in the PAZ. The uptake rates of the different N forms were not significantly correlated with one another or with the ambient N concentrations (Table S1).

Ammonium oxidation rates ( $\text{NH}_4^+_{\text{ox}}$ ) increased southwards, with higher  $\text{NH}_4^+_{\text{ox}}$  in the OAZ and PAZ than in the STZ, SAZ, and PFZ (Fig. 5c).  $\text{NH}_4^+_{\text{ox}}$  was generally comparable to previous wintertime measurements from the surface of the open Southern Ocean (Mdutyana et al., 2020).  $\text{NH}_4^+_{\text{ox}}$  was not correlated with the ambient  $\text{NH}_4^+$  concentration (Table S1).

#### 4.5 Plankton community composition

Microplankton abundance was low, with the highest cell counts recorded at stations 37.2°S and 41.3°S in the STZ and no cells counted at 38.1°S (STZ) and 55.5°S (OAZ) (Fig. 6a). On average, microplankton abundance was higher in the STZ than in the SAZ, PFZ, and OAZ. The greatest diversity of microplankton groups was observed at 41.3°S in the STZ and at 50.0°S near the PF.

Centric diatoms (including *Planktoniella*, *Coscinodiscus*, and *Thalassiosira* species) were detected only at the southernmost station 58.9°S (3 cells mL<sup>-1</sup>). Pennate diatoms (including *Pseudo-nitzschia*, *Pleurosigma*, and *Navicula* species) were more abundant in the STZ, PFZ, and OAZ, with negligible abundances in the SAZ. Higher pennate diatom abundances occurred near the PF (7 cells mL<sup>-1</sup>), as has been observed in summer (e.g., Bracher et al., 1999). Dinoflagellates were identified at every station except 38.1°S and were most abundant in the STZ and PFZ. At all but three stations, small (~15 µm) dinoflagellates were the most abundant group, although the larger *Protoperidinium* dinoflagellate species (mainly heterotrophic; Jeong & Latz, 1994) were almost as abundant in the PFZ and at 54.0°S. Microzooplankton (i.e., ciliates, 20-200 µm) were most abundant in the STZ, and were also present in the PFZ at 46.1°S (3 cells mL<sup>-1</sup>) and 48.9°S (3 cells mL<sup>-1</sup>) and in the OAZ at 50.0°S (1 cells mL<sup>-1</sup>) and 54.0°S (4 cells mL<sup>-1</sup>). All other stations were characterized by negligible (<1 cells mL<sup>-1</sup>) microzooplankton abundances.

Nano- and picoeukaryotes, *Synechococcus*, and heterotrophic bacteria (collectively, “small cells”) were roughly 10<sup>3</sup>-times more abundant than the microplankton (Fig. 6b). Notwithstanding a lack of data from the STZ, the highest small cell abundances occurred in the SAZ near the SAF. Across the transect, picoeukaryotes were generally more abundant than all other phytoplankton groups (average picoeukaryote contribution to total small cells of 12-54%; nanoeukaryotes of 7-39%; *Synechococcus* of 15-42%). A similar trend has been observed for the Southern Ocean in spring (Detmer & Bathmann, 1997) and late summer (Fiala et al., 1998), in contrast to mid-summer observations showing nanoplankton dominance (e.g., Ishikawa et al., 2002; Weber & El-Sayed, 1987). Additionally, picoeukaryotes were two- to three orders of magnitude more abundant in the SAZ and PFZ than in the OAZ. Nanoeukaryotes dominated near the PF at 50.0°S (39%) and in the southern OAZ at 55.5°S (36%), while *Synechococcus* dominated at 42.7°S and 54.0°S (42% and 33%, respectively). In general, nanoeukaryote abundance was higher in the SAZ than in the PFZ and OAZ, as was that of *Synechococcus*.

The contribution of heterotrophic bacteria to total small cells varied considerably (10-62%), reaching a maximum south of the PF at 53.0°S and 57.8°S (62% and 50%), and with higher abundances in the SAZ than in the PFZ and OAZ (Fig. 7). Additionally, heterotrophic bacterial abundances were ten-fold lower to two-fold higher than the total pico- and nanophytoplankton cell counts. Detrital particles were most abundant near the southern edge of the SAF, and were generally more abundant in the PFZ than in the SAZ and OAZ (Fig. S5).

#### 4.6 2018/19 cruises: ammonium concentrations

In early summer, surface NH<sub>4</sub><sup>+</sup> concentrations were uniformly low across the transect (average of 0.11 ± 0.09 µM; Fig. 8a). South of the SAF, NH<sub>4</sub><sup>+</sup> increased to an average concentration of 0.81 ± 0.92 µM by late summer (Fig. 8b). By winter 2019, the NH<sub>4</sub><sup>+</sup> concentrations south of the SAF were ~40% lower than they had been in late summer (Fig. 8c), and were similar to those

486 observed in winter 2017 ( $0.50 \pm 0.30 \mu\text{M}$  and  $0.52 \pm 0.11 \mu\text{M}$ , respectively), confirming that our  
 487 2017 observations are generally representative of the wintertime Southern Ocean. By early  
 488 spring, the  $\text{NH}_4^+$  concentrations south of the SAF had declined to near or below detection ( $0.09$   
 489  $\pm 0.08 \mu\text{M}$ ; Fig. 8d) before rising again by late spring to an average value only slightly lower  
 490 than that measured in winter ( $0.40 \pm 0.74 \mu\text{M}$ ; Fig. 8e). However, the late-spring  $\text{NH}_4^+$   
 491 concentrations were only elevated in the PFZ (range of  $0.11 \pm 0.01$  to  $4.39 \pm 0.03 \mu\text{M}$ , average  
 492 of  $0.77 \pm 1.11 \mu\text{M}$ ), as has been observed previously (Bathmann et al., 1997). Excluding the PFZ  
 493 data yields a far lower late-spring average of  $0.17 \pm 0.11 \mu\text{M}$  south of the SAF, which we take  
 494 as more broadly representative of this season.

#### 495 4.7 Mixed-layer $\text{NH}_4^+$ residence time and $\text{NH}_4^+$ production rate estimates

496 The  $\text{NH}_4^+$  residence time in winter 2017, computed using Eqn 5, ranged from 10 to 38 days (median  
 497 of 21 days) south of the SAF and from 0 to 6 days (median of 2 days) north of the SAF. These  
 498 values were estimated using wintertime measurements only and as such, may not be  
 499 representative of the transition from summer to winter. To refine our estimates, we used average  
 500  $\text{pNH}_4^+$  and  $\text{NH}_4^+$  concentration measurements. South of the SAF in late summer,  $\text{pNH}_4^+ = 50.6 \pm$   
 501  $24.0 \text{ nM day}^{-1}$  and the  $\text{NH}_4^+$  concentration =  $0.81 \pm 0.92 \mu\text{M}$  (Deary, 2020), which together yield  
 502 an  $\text{NH}_4^+$  residence time of 2 to 27 days (median of 5 days). The  $\text{NH}_4^+$  residence time north of the SAF,  
 503 calculated using  $\text{pNH}_4^+ = 20.7 \pm 8.6 \text{ nM day}^{-1}$  and  $\text{NH}_4^+$  concentration =  $0.16 \pm 0.45 \mu\text{M}$  (Deary,  
 504 2020) was 1 to 17 days (median of 14 days).

505 The  $\text{NH}_4^+$  production rate south of the SAF, calculated using Eqn 8 and an  $[\text{NH}_4^+]_{\text{decline}}$  of 330 nM (i.e.,  
 506 the difference between late summer and winter 2019;  $810 \text{ nM} - 480 \text{ nM}$ ),  $t$  of 141 days, and  
 507  $\text{NH}_4^+$  removal rate of  $50.6 \pm 24.0 \text{ nM day}^{-1}$  (here, the average late-summer  $\text{pNH}_4^+$  south of the SAF is  
 508 used to approximate  $\text{NH}_4^+$  removal rate), was  $52.9 \pm 25.0 \text{ nM day}^{-1}$ . Similarly, north of the SAF (using  
 509 an  $[\text{NH}_4^+]_{\text{decline}}$  of 20 nM, i.e.,  $160 \text{ nM} - 140 \text{ nM}$ , and  $\text{NH}_4^+$  removal rate of  $20.7 \pm 8.6 \text{ nM day}^{-1}$ ), the  
 510  $\text{NH}_4^+$  production rate was  $50.7 \pm 9.3 \text{ nM day}^{-1}$ . If we instead use the average  $\text{NH}_4^+$  removal rate and  $\text{NH}_4^+$   
 511 concentration measured in winter 2017 south ( $21.4 \pm 0.6 \text{ nM day}^{-1}$  and  $520 \pm 110 \text{ nM}$ ) and north  
 512 ( $18.4 \pm 0.8 \text{ nM day}^{-1}$  and  $80 \pm 10 \text{ nM}$ ) of the SAF, the  $\text{NH}_4^+$  production rate was  $23.4 \pm 6.6 \text{ nM day}^{-1}$   
 513 and  $18.5 \pm 6.6 \text{ nM day}^{-1}$ , respectively. Using the range of  $\text{NH}_4^+$  removal rate estimates and the average  
 514 ambient  $\text{NH}_4^+$  concentration measured south of the SAF in winter 2017 ( $16.7$  to  $31.2 \text{ nM day}^{-1}$   
 515 and  $520 \text{ nM}$ ) and late summer 2019 ( $22.6$  to  $98.6 \text{ nM day}^{-1}$  and  $810 \text{ nM}$ ), we calculate that over  
 516 the late-summer-to-winter transition, the  $\text{NH}_4^+$  production rate ranged from  $18.8$  to  $100.9 \text{ nM day}^{-1}$   
 517 (compared to  $6.3$  to  $28.8 \text{ nM day}^{-1}$  north of the SAF).

## 518 5. Discussion

### 519 5.1 Drivers of $\text{NH}_4^+$ cycling in the surface layer of the Southern Ocean

521 Previous work has suggested that  $\text{NH}_4^+$  accumulates in the Southern Ocean mixed layer following  
 522 the late summer increase in heterotrophy, then decreases into autumn as heterotrophic activity  
 523 subsides, to be depleted by winter due to advective processes and biological removal (Koike et  
 524 al., 1986; Serebrennikova & Fanning, 2004). However, our data show that  $\text{NH}_4^+$  concentrations  
 525 are elevated in the mixed layer in winter, particularly south of the SAF (Fig. 2). Similarly elevated  
 526 winter surface-layer  $\text{NH}_4^+$  has been observed previously in both the Atlantic and Indian sectors,

Deleted: south of the SAF

Deleted: and from 0 to 6 days (median of 2 days)

Deleted: and north

Deleted: , respectively

Deleted: the

Deleted: measured

Deleted: south

Deleted: (

Deleted: ,

Deleted: respectively;

Deleted: s

Deleted: the average

Deleted: measured north of the SAF in late summer

Deleted:  $20.7 \pm 8.6 \text{ nM day}^{-1}$  and  $0.16 \pm 0.45 \mu\text{M}$ ,  
 respectively; ...

Deleted: ,

Deleted: 0.16

Deleted: 0.14

Deleted: of

Formatted: Superscript

Formatted: Not Superscript/ Subscript

Deleted:

Deleted: values

Formatted: Not Superscript/ Subscript

Deleted: The  $\text{NH}_4^+$  residence time in winter 2017 south of the  
 SAF, computed using Eqn 5, ranged from 10 to 38 days  
 (median of 21 days). These values were estimated using  
 wintertime measurements only and as such, may not be  
 representative of the transition from summer to winter. To  
 refine our estimates, we use the average  $\text{pNH}_4^+$  and  $\text{NH}_4^+$   
 concentration measured south of the SAF in late summer  
 ( $50.6 \pm 24.0 \text{ nM day}^{-1}$  and  $0.81 \pm 0.92 \mu\text{M}$ , respectively;  
 Deary, 2020), which yields an  $\text{NH}_4^+$  residence time of 2 to 27 days  
 (median of 5 days).

The  $\text{NH}_4^+$  production rate, calculated using Eqn 8 and an  
 $[\text{NH}_4^+]_{\text{decline}}$  of 330 nM (i.e.,  $810 \text{ nM} - 480 \text{ nM}$ ),  $t$  of 141  
 days, and  $\text{NH}_4^+$  removal rate of  $50.6 \pm 24.0 \text{ nM day}^{-1}$  (here,  
 the average late-summer  $\text{pNH}_4^+$  south of the SAF is used to  
 approximate  $\text{NH}_4^+$  removal rate), was  $52.9 \pm 25.0 \text{ nM day}^{-1}$ . If we  
 instead use the average  $\text{NH}_4^+$  removal rate and  $\text{NH}_4^+$  concentration  
 measured in winter 2017 ( $21.4 \pm 0.6 \text{ nM day}^{-1}$  and  $520 \pm 110$   
 nM), the  $\text{NH}_4^+$  production rate was  $23.4 \pm 6.6 \text{ nM day}^{-1}$ . Using the  
 range of  $\text{NH}_4^+$  removal rate values and the average ambient  $\text{NH}_4^+$   
 concentration measured south of the SAF in winter 2017  
 ( $16.7$  to  $31.2 \text{ nM day}^{-1}$  and  $520 \text{ nM}$ ) and late summer 2019  
 ( $22.6$  to  $98.6 \text{ nM day}^{-1}$  and  $810 \text{ nM}$ ), we calculate that over  
 the late-summer-to-winter transition, the  $\text{NH}_4^+$  production rate  
 ranged from  $18.8$  to  $100.9 \text{ nM day}^{-1}$ .

with concentrations typically increasing towards the south (Philibert et al., 2015; Mdutyana et al., 2020; Bianchi et al., 1997). Numerous overlapping processes are likely involved in setting the ambient  $\text{NH}_4^+$  concentrations, as summarized in Fig. 9. In this study, we directly measured the rates of  $\text{NH}_4^+$  uptake and oxidation, and estimated the rates of  $\text{NH}_4^+$  production, along with qualitatively evaluating the role of heterotrophy from the relative abundance of heterotrophic bacteria, phytoplankton, and detritus. For the  $\text{NH}_4^+$  cycle processes shown in Fig. 9 that are not quantified or inferred from our dataset, we consider their potential role in Southern Ocean  $\text{NH}_4^+$  cycling based on findings reported in the literature.

The high  $\text{NH}_4^+$  concentrations observed south of the SAF in winter may result from net  $\text{NH}_4^+$  accumulation during late summer, autumn, and/or winter. The persistence of elevated  $\text{NH}_4^+$  concentrations that are near-homogeneously distributed throughout the mixed layer is consistent with a residence time for the winter  $\text{NH}_4^+$  reservoir in excess of the time-scale for upper-ocean mixing. Indeed, we calculate a median residence time of 21 days south of the SAF, compared to 2 days north of the SAF. One implication of the long residence time computed for the polar zones is that the wintertime  $\text{NH}_4^+$  pool likely reflects both ongoing processes and those that occurred earlier in the year. We posit that the elevated  $\text{NH}_4^+$  concentrations south of the SAF may result from higher wintertime rates of  $\text{NH}_4^+$  production than removal and/or from the gradual but incomplete depletion in winter of  $\text{NH}_4^+$  produced mainly in late summer and autumn. We evaluate both possibilities throughout the discussion below.

#### 5.1.1 Ammonium removal

*Ammonium assimilation* – Microbial growth is limited in the winter Southern Ocean (Arrigo et al., 2008; Smith Jr et al., 2000; Takao et al., 2012), resulting in low cell abundances and nutrient uptake rates (Church et al., 2003; Iida & Odate, 2014; Mdutyana et al., 2020). However, while the concentrations of chl-a and rates of NPP were low across our transect, they were not negligible (Fig. 3a and 5a), consistent with previous reports for this season (Mordy et al., 1995; Pomeroy & Wiebe, 2001). Southern Ocean phytoplankton are adapted to survive suboptimal conditions; for example, numerous species achieve their maximum growth rates at temperatures that are considerably lower than the optimal growth temperatures of temperate and tropical species (2-9 °C versus 10-30 °C and 15-35 °C, respectively), with sharp declines in growth rates observed at temperatures outside this range (Boyd et al., 2013; Coello-Camba & Agusti, 2017; Fiala & Oriol, 1990). In addition, ice-free Southern Ocean waters typically extend to <60°S in the eastern Atlantic and western Indian sectors in winter, so that even though irradiance levels may not be optimal for phytoplankton growth, there is always some light available for photosynthesis. The hostile wintertime conditions of the open Southern Ocean do not, therefore, prevent ecosystem functioning, although the microbial dynamics and associated biogeochemical processes differ from those occurring in summer (Smart et al., 2015; Mdutyana et al., 2020).

We measured fairly low surface  $\text{NH}_4^+$  uptake rates (3.0-13.2 nM day<sup>-1</sup>; Fig. 5b) compared to previous wintertime observations (ranging from 32-66 nM day<sup>-1</sup>; Cota et al., 1992; Mdutyana et al., 2020; Philibert et al., 2015). Such low rates, if generally representative of winter, would limit mixed-layer  $\text{NH}_4^+$  drawdown, especially south of the PF where  $\rho\text{NH}_4^+$  was particularly low. Recycled N ( $\text{NH}_4^+$  + urea) nonetheless accounted for most of the N assimilated during winter, including in the AZ (Fig. 5b).

The available  $\delta^{15}\text{N}$ -PON data suggest that the preferential reliance of phytoplankton on recycled N may have persisted from the late summer. In theory, PON generated in early- through mid-summer from the assimilation of upwelled  $\text{NO}_3^-$  ( $\delta^{15}\text{N}$ - $\text{NO}_3^-$  of 5.2‰ in the AZ and 6.2‰ in the SAZ; Smart et al., 2015; Fripiat et al., 2019; 2021) will have a  $\delta^{15}\text{N}$  of ~0‰ in the AZ and 1-2‰ in the SAZ given the isotope effect of  $\text{NO}_3^-$  assimilation and the degree of seasonal  $\text{NO}_3^-$  drawdown (Sigman et al., 1999; Granger et al., 2004; 2010). Such  $\delta^{15}\text{N}$ -PON values have indeed been measured in the early- and mid-summer Southern Ocean (Lourey et al., 2003; Smart et al., 2020; Soares et al., 2015). By late summer,  $\delta^{15}\text{N}$ -PON has been observed to decline to between -5 and -1‰, with the lowest values occurring in the AZ (Lourey et al., 2003; Smart et al., 2020; Trull et al., 2008). Since the  $\delta^{15}\text{N}$  of recycled N is expected to be low (<0‰; Checkley & Miller, 1989; Macko et al., 1986), the early-to-late summer decline in  $\delta^{15}\text{N}$ -PON implicates a switch from dominantly  $\text{NO}_3^-$  to dominantly recycled N-supported phytoplankton growth (Lourey et al., 2003). For the SAZ, the subsequent late summer-to-winter rise in  $\delta^{15}\text{N}$ -PON (i.e., from ~ -1‰ to 1-2.5‰; Fig. 4) has previously been attributed to PON decomposition by heterotrophic bacteria (Smart et al., 2020), during which  $^{14}\text{N}$ - $\text{NH}_4^+$  is preferentially remineralized, leaving the remaining PON enriched in  $^{15}\text{N}$  (Möbius, 2013). That  $\text{NH}_4^+$  concentrations are not elevated in the SAZ mixed layer in winter (Fig. 2b) indicates that the remineralized  $\text{NH}_4^+$  is rapidly re-assimilated by phytoplankton and/or oxidized to  $\text{NO}_2^-$  in this zone. In the AZ, the much lower  $\delta^{15}\text{N}$ -PON of -3 to -1‰ that we observe in winter surface waters requires the sustained assimilation of low- $\delta^{15}\text{N}$  N (i.e., recycled N) to offset a remineralization-driven  $\delta^{15}\text{N}$  rise akin to that of the SAZ. We conclude that Southern Ocean phytoplankton preferentially consume regenerated N from late summer until at least July (albeit at low rates in winter), particularly south of the PF.

The fact that  $\text{NH}_4^+$  accumulated in the winter mixed layer despite being the preferred phytoplankton N source in late summer through winter implies that low rates of  $\text{NH}_4^+$  uptake contributed to its accumulation. Multiple factors may cause low rates of photoautotrophic  $\text{NH}_4^+$  assimilation, including deplete  $\text{NH}_4^+$  and micronutrient concentrations, light limitation, and low temperatures. North of the SAF,  $\text{NH}_4^+$  concentrations below detection likely limited  $\text{pNH}_4^+$ , as evidenced by the fact that in a series of experiments conducted on the same cruise,  $\text{pNH}_4^+$  increased with the addition of  $\text{NH}_4^+$  at these stations (Mdutyana, 2021). By contrast, south of the SAF,  $\text{NH}_4^+$  concentrations were similar to or higher than the half-saturation constant ( $K_m$ ) derived for  $\text{NH}_4^+$  uptake in the winter Southern Ocean (0.2 to 0.4  $\mu\text{M}$ ; Mdutyana, 2021), suggesting that something other than  $\text{NH}_4^+$  availability was limiting to phytoplankton at these latitudes.

Iron is not directly involved in  $\text{NH}_4^+$  assimilation but is required for electron transport during photosynthesis and respiration, as well as for chlorophyll synthesis (Raven, 1988). While iron limitation is widespread across the Southern Ocean (Janssen et al., 2020; Pausch et al., 2019; Viljoen et al., 2019), iron availability appears to be higher in winter than during other seasons (Mtshali et al., 2019; Tagliabue et al., 2014) due to enhanced mixing, storms, and increased aeolian deposition (Coale et al., 2005; Honjo et al., 2000; Sedwick et al., 2008). The fact that  $\text{pNO}_3^-$  and  $\text{pNH}_4^+$  were generally similar across the transect (Fig. 5b) argues against a dominant role for iron in controlling  $\text{pNH}_4^+$  since  $\text{NO}_3^-$  consumption has a far higher iron requirement than  $\text{NH}_4^+$  assimilation (Morel et al., 1991).

Deleted: assimilation



657 In contrast to  $\text{NH}_4^+$  and iron availability, light limitation is exacerbated in winter due to low  
 658 insolation, increased cloud-cover, and mixed layers that can be hundreds of meters deeper than  
 659 the euphotic zone (Buongiorno Nardelli et al., 2017; Sallée et al., 2010). Light is thus often  
 660 considered the dominant constraint on Southern Ocean primary productivity in this season  
 661 (Thomalla et al., 2011; Lloret et al., 2019; Wadley et al., 2014). However, since  $\text{NH}_4^+$  assimilation  
 662 by phytoplankton is fairly energetically inexpensive (Dortch, 1990), it should occur even under  
 663 low light conditions (recognizing that light remains critical for coincident  $\text{CO}_2$  fixation).  
 664 Heterotrophic bacteria can also consume  $\text{NH}_4^+$  (Kirchman, 1994), including in the dark, as they  
 665 derive energy from organic carbon oxidation rather than light. At an ecosystem level, therefore,  
 666  $\text{NH}_4^+$  assimilation may not be primarily limited by light, although this parameter clearly strongly  
 667 controls the rate and distribution of NPP (Fig. 5a).

668 Previous observations suggest that temperature can influence  $\text{NH}_4^+$  uptake, especially in winter  
 669 (Glibert, 1982; Reay et al., 2001). The negative effect of temperature appears to be enhanced  
 670 under high-nutrient and low-light conditions, at least in the case of phytoplankton growth rates  
 671 (Baird et al., 2001). Experiments conducted coincident with our sampling showed that the  
 672 maximum rate of  $\text{NH}_4^+$  uptake ( $V_{\text{max}}$ ) achievable by the *in situ* community was strongly  
 673 negatively correlated with temperature and latitude (Mdutyana, 2021), with the latter parameter  
 674 representing the combined role of light, temperature, and possibly iron, the average concentration  
 675 of which appears to increase from the SAZ to the AZ (Tagliabue et al., 2012). We conclude that  
 676 these three drivers, along with  $\text{NH}_4^+$  availability north of the SAF, may all play a role in  
 677 controlling photoautotrophic  $\text{NH}_4^+$  assimilation in the winter Southern Ocean, with complex  
 678 interactions among them that are difficult to disentangle.

679 In addition to physical and chemical limitations, microbial preference for other N species may  
 680 impact  $\text{NH}_4^+$  depletion. For example, the preferential uptake of urea and/or other dissolved  
 681 organic N (DON) species by some organisms (e.g., picoeukaryotes, cyano- or heterotrophic  
 682 bacteria) could cause a net decrease in the total  $\text{NH}_4^+$  uptake rates. While urea has been shown to  
 683 constitute a large fraction of the total N assimilated by Southern Ocean phytoplankton in summer  
 684 and autumn (albeit mainly in the SAZ; Joubert et al., 2011; Thomalla et al., 2011), we measured  
 685 fairly low  $\rho\text{Urea}$  (Fig. 5b), which is perhaps unsurprising given the low ambient urea  
 686 concentrations (Table 1). The exceptions were stations 37°S and 43.0°S where  $\rho\text{Urea}$  was higher  
 687 than  $\rho\text{NH}_4^+$ , coincident with very low ambient  $\text{NH}_4^+$  (0.10  $\mu\text{M}$  and below detection) and relatively  
 688 high urea concentrations (0.36  $\mu\text{M}$  and 0.15  $\mu\text{M}$ , respectively).

689 Community composition can also alter the N uptake regime. Small phytoplankton, such as the  
 690 numerically-dominant nano- and picoeukaryotes, are more likely to consume  $\text{NH}_4^+$  and urea than  
 691  $\text{NO}_3^-$  (Koike et al., 1986; Lee et al., 2012; 2013), especially under conditions of iron and light  
 692 limitation (Sunda & Huntsman, 1997). Across our transect, reduced N (i.e.,  $\text{NH}_4^+$  + urea) uptake  
 693 exceeded  $\text{NO}_3^-$  uptake for both the total phytoplankton community (transect average of  $12.0 \pm$   
 694  $0.9 \text{ nM day}^{-1}$  for reduced N versus  $5.8 \pm 1.0 \text{ nM day}^{-1}$  for  $\text{NO}_3^-$ ; f-ratio of 0.36) and the pico size  
 695 fraction ( $5.0 \pm 1.2 \text{ nM day}^{-1}$  versus  $1.9 \pm 1.2 \text{ nM day}^{-1}$ ; f-ratio of 0.27; Fig. 5b). That said, the  
 696  $\text{NO}_3^-$  uptake rates were not negligible, including in the pico size fraction. In the PFZ and AZ,  
 697  $\text{NO}_3^-$  uptake by the picoplankton was far more strongly correlated with the abundance of  
 698 picoeukaryotes than *Synechococcus* ( $r = 0.75$  and  $0.03$ , respectively), consistent with  
 699 observations of dominant reliance on  $\text{NO}_3^-$  by picoeukaryotes and  $\text{NH}_4^+$  by *Synechococcus* in

Deleted: severe



other ocean regions (Fawcett et al., 2011; 2014; Painter et al., 2014). Additionally, *Synechococcus* abundance was strongly correlated with  $\text{NH}_4^+$  concentration south of the SAF ( $r = 0.65$ ). In the nano+ size class,  $\text{NO}_3^-$  uptake was likely driven in the SAZ by dinoflagellates and nanoeukaryotes, and in the PFZ and AZ by diatoms, which remain active in these zones in winter (Weir et al., 2020). By contrast, nanoeukaryotes, which have a higher per-cell nutrient requirement than the equally-abundant picoeukaryotes, may have dominated  $\text{NH}_4^+$  uptake in the PFZ and AZ given that higher nanoeukaryote abundances corresponded with lower  $\text{NH}_4^+$  concentrations at a number of stations (e.g., stations 50.0°S, 51.1°S, and 55.5°S; Fig. 6b).

The low abundances of diatoms and dinoflagellates and absence of coccolithophores across our transect (Fig. 6a) is expected given the limitations imposed on nutrient uptake and  $\text{CO}_2$  fixation by winter Southern Ocean conditions. The lower surface area-to-volume ratio of large cells means that they rapidly experience diffusion-limitation of  $\text{NH}_4^+$  and micronutrient uptake and are more susceptible to light limitation (Finkel et al., 2004), resulting in their being outcompeted by smaller species for essential resources (Franck et al., 2005; Cavender-Bares et al., 1999). The near-absence of centric diatoms is also best explained thus, particularly given their low surface area-to-volume ratio compared to the more-abundant pennate species (Kobayashi & Takahashi, 2002) that are more likely to consume  $\text{NH}_4^+$  (Semeneh et al., 1998). Diatom success in winter may also be limited by enhanced mixing, as this group generally prefers stratified waters (Kopczynska et al., 2007).

In sum,  $\text{NH}_4^+$  uptake rates were low across our transect but not negligible, indicating that phytoplankton activity in winter, which is dominated by smaller species, is a sink for  $\text{NH}_4^+$ . The hostile conditions of the winter Southern Ocean imposed limitations on  $\text{NH}_4^+$  uptake that varied with latitude, with  $\text{NH}_4^+$  concentrations controlling  $\text{pNH}_4^+$  north of the SAF, while light and temperature were important south of the SAF. Additionally, *Synechococcus*, nanoeukaryotes, and pennate diatoms likely dominated  $\text{NH}_4^+$  assimilation, consistent with previous observations from the Southern Ocean and elsewhere (Klawonn et al., 2019; Semeneh et al., 1998).

*Ammonium oxidation* – Nitrification removes more mixed-layer  $\text{NH}_4^+$  in winter than phytoplankton assimilation south of the PF, with  $\text{NH}_4^+$  oxidation rates that were two- to five-times the co-occurring  $\text{NH}_4^+$  uptake rates (Fig. 5c). The comparative success of ammonia oxidisers may be due to decreased competition with phytoplankton for  $\text{NH}_4^+$ , augmented by decreased photoinhibition (Wan et al., 2018; Lu et al., 2020), elevated  $\text{NH}_4^+$  availability (Baer et al., 2014; Mdutyana et al., 2020; Mdutyana, 2021), and the **apparently minor** effect of temperature on  $\text{NH}_4^+$  oxidation (Bianchi et al., 1997; Baer et al., 2014; Horak et al., 2013; Mdutyana 2021). One implication of the dominance of  $\text{NH}_4^+$  oxidation in winter is that in addition to the limitations on photoautotrophic  $\text{NH}_4^+$  assimilation discussed above, low phytoplankton success in the AZ may result from nitrifiers outcompeting phytoplankton for scarce resources (e.g., trace elements required for enzyme functioning, such as iron and copper; Amin et al., 2013; Maldonado et al., 2006; Shafiee et al., 2019) under conditions of low incident light and enhanced mixing.

The  $K_m$  derived for  $\text{NH}_4^+$  oxidation in the winter Southern Ocean has recently been reported to be low (0.03 to 0.14  $\mu\text{M}$ ), with ammonia oxidizers observed to become saturated at ambient  $\text{NH}_4^+$  concentrations of  $\sim 0.1\text{--}0.2 \mu\text{M}$  (Mdutyana, 2021). This means that south of the SAF in winter 2017, ammonia oxidizers were not substrate limited (as implied by the lack of correlation

Deleted: ,

Deleted: minimal

between  $\text{NH}_4^+_{\text{ox}}$  and  $\text{NH}_4^+$  concentration; Table S1), which raises the question of why  $\text{NH}_4^+$  oxidation did not occur at higher rates. The answer may indirectly involve temperature, in that psychrophilic organisms can be less responsive to high substrate concentrations at low temperatures (Baer et al., 2014). Another possibility is that  $\text{NH}_4^+$  oxidation was iron-limited (Shiozaki et al., 2016; Shafiee et al., 2019; Mdutyana, 2021). In any case, ammonia oxidisers were moderately successful across the surface Southern Ocean in winter, with low light, reduced competition with phytoplankton, and substrate repletion likely explaining the elevated  $\text{NH}_4^+$  oxidation rates south of the PF compared to the stations to the north.

#### 5.1.2 Ammonium production and other sources of ammonium

$\text{NH}_4^+$  production must have been sustained during the winter to maintain a mixed-layer  $\text{NH}_4^+$  pool south of the SAF that was high in concentration relative to the early summer. Indeed, the residence time estimated for  $\text{NH}_4^+$  in winter (10 to 38 days) is considerably shorter than the transition from late summer to winter (approximately three months), indicating that heterotrophic  $\text{NH}_4^+$  production, which would have occurred coincident with  $\text{NH}_4^+$  consumption, must have been ongoing in winter. We estimate the rate of this wintertime  $\text{NH}_4^+$  production to be  $23.4 \pm 6.6$   $\text{nM day}^{-1}$ .

*Heterotrophic activity by bacteria* – Heterotrophic bacteria contribute significantly to  $\text{NH}_4^+$  production in the Southern Ocean (Hewes et al., 1985; Koike et al., 1986; Tréguer & Jacques, 1992), including in winter (Rembauville et al., 2017). In our dataset, lower ratios of photosynthetic-to-heterotrophic cells were observed at stations with higher  $\text{NH}_4^+$  concentrations (e.g., stations 48.9°S, 53.0°S, 54.0°S, and 57.8°S; Fig. S5a), consistent with a role for the heterotrophic bacteria present at the time of sampling in generating the ambient  $\text{NH}_4^+$  pool. The potential for ongoing heterotrophic activity can also be inferred from the high detrital particle counts along the transect (Fig. 7). However, since heterotrophic bacteria are likely more active in late summer and autumn when the temperature and the supply of labile PON are higher (Becquevort et al., 2000; Dennett et al., 2001; Pomeroy & Wiebe, 2001; Smart et al., 2020), we expect that the winter  $\text{NH}_4^+$  pool includes  $\text{NH}_4^+$  produced in late summer and autumn. A further consideration is assimilation of  $\text{NH}_4^+$  by heterotrophic bacteria, reported to occur at elevated rates in the Southern Ocean mixed layer in winter (Mdutyana et al. 2020; Text S3). If this process is a persistent feature of the winter Southern Ocean, it will decrease the net contribution of heterotrophic bacteria to  $\text{NH}_4^+$  accumulation. We conclude that it is unlikely that the surface  $\text{NH}_4^+$  pool measured in winter derived solely from wintertime bacterial  $\text{NH}_4^+$  production given that yet higher  $\text{NH}_4^+$  concentrations have been observed in late summer and autumn (Becquevort et al., 2000; Dennett et al., 2001), including in the present study (see section 5.2 below).

*Heterotrophic activity by zooplankton* – While the microzooplankton enumerated in this study occurred at very low abundances, those that were present likely contributed to the  $\text{NH}_4^+$  flux. For example, at stations 48.9°S and 54.0°S in the PFZ and AZ, respectively, both the ratios of photosynthetic-to-heterotrophic cells and the absolute abundances of heterotrophic bacteria were low, while the microzooplankton abundances and  $\text{NH}_4^+$  concentrations were elevated compared to nearby stations. The implication of these observations is that elevated microzooplankton abundances may help to explain high  $\text{NH}_4^+$  concentrations in waters with low numbers of heterotrophic bacteria, although we note that this scenario only occurred at two stations. On

Deleted: 7

Deleted: b

balance, we posit that microzooplankton are less important for wintertime  $\text{NH}_4^+$  production than heterotrophic bacteria given their low abundances in the surface layer (Fig. 6a; Atkinson et al., 2012). That said, it is possible that the contribution of micro- (and/or macro-) zooplankton to the  $\text{NH}_4^+$  pool surpasses that of heterotrophic bacteria under certain conditions (Koike et al., 1986; Priddle et al., 1998), such as in (late) summer and near regions of frontal upwelling in response to elevated rates of phytoplankton biomass accumulation.

Above, we have assumed that  $\text{NH}_4^+$  production is the direct result of heterotrophy. However, there are other possible mechanisms of  $\text{NH}_4^+$  supply that should be considered. We briefly address some of these processes below, noting that for most, there are very few to no observations available from the Southern Ocean.

*DON cycling* –  $\text{NH}_4^+$  can be released by heterotrophic bacteria that directly consume DON (e.g., urea; Billen, 1983; Tupas & Koike, 1990), and possibly also by ammonia oxidisers that convert DON to  $\text{NH}_4^+$  intracellularly, through the equilibration of the intra- and extracellular  $\text{NH}_4^+$  pools (Kitzinger et al., 2019). DON can also be converted to  $\text{NH}_4^+$  through photodegradation by UV radiation (e.g., Aarnos et al., 2012). Bacterial decomposition of DON (rather than PON) to  $\text{NH}_4^+$  is implicit in most estimates of ammonification, however, and cellular  $\text{NH}_4^+$  efflux by ammonia oxidisers is likely extremely low given that they require  $\text{NH}_4^+$  to fix  $\text{CO}_2$ . Additionally, the low light flux to the surface Southern Ocean in winter means that photodegradation will not yield a significant supply of  $\text{NH}_4^+$ . Thus, DON conversion to  $\text{NH}_4^+$ , through any mechanism, is probably negligible.

*External inputs of ammonium* – High surface ocean  $\text{NH}_4^+$  concentrations may theoretically derive from external inputs of  $\text{NH}_4^+$ , such as  $\text{N}_2$  fixation,  $\text{NH}_4^+$  aerosol deposition, or sea-ice melt.  $\text{N}_2$  fixation should be below detection in the winter Southern Ocean due to the cold temperatures, low light and iron conditions, and high  $\text{NO}_3^-$  concentrations (Jiang et al., 2018; Knapp et al., 2012; Kustka et al., 2003).  $\text{NH}_4^+$  aerosols are unlikely to be abundant over regions of the Southern Ocean remote from islands and coastal Antarctica, particularly in winter when  $\text{NH}_4^+$  aerosol concentrations have been shown to reach a minimum (Legrand et al., 1998; Xu et al., 2019). Moreover, the aerosols that are present over the open Southern Ocean will derive mainly from surface-ocean  $\text{NH}_3$  efflux; once re-deposited, this  $\text{NH}_4^+$  does not constitute a new input to surface waters (Altieri et al., 2021). Finally, since our sampling took place before the sea-ice reached its northernmost extent (Cavaliere & Parkinson, 2008), the dominant process would have been sea-ice formation rather than sea-ice melt, the latter an occasional source of  $\text{NH}_4^+$  (Kattner et al., 2004; Zhou et al., 2014). In any case, we observed elevated  $\text{NH}_4^+$  concentrations as far north as  $46^\circ\text{S}$ , ~1700 km beyond the influence of sea-ice melt.

## 5.2 Seasonal cycling of $\text{NH}_4^+$ in the Southern Ocean mixed layer south of the SAF

The  $\text{NH}_4^+$  concentration data collected over the 2018/19 annual cycle provide context for interpreting our winter 2017 dataset, allowing us to address our hypothesis that  $\text{NH}_4^+$  production in late summer and autumn contributes to the elevated  $\text{NH}_4^+$  concentrations measured in winter.

The very low  $\text{NH}_4^+$  concentrations observed in early summer (Fig. 8a) are consistent with high rates of phytoplankton  $\text{NH}_4^+$  assimilation during the spring and early-summer growing period (Mdutyana et al., 2020; Savoye et al., 2004; Daly et al., 2001). By late summer, the  $\text{NH}_4^+$

concentrations increased (Fig. 8b) presumably due to elevated heterotrophic activity (i.e., bacterial decomposition and zooplankton grazing) following the accumulation of algal biomass (Mengesha et al., 1998; Le Moigne et al., 2013), coupled with iron- and/or silicate-limitation of phytoplankton (Hiscock et al., 2003; Sosik & Olson, 2002) and enhanced grazing pressure (Becquevort et al., 2000). Mixed-layer  $\text{NH}_4^+$  remained high between late summer and winter (Fig. 8b-c), likely due to sustained heterotrophic  $\text{NH}_4^+$  production in excess of  $\text{NH}_4^+$  removal. This notion is supported by estimates of the residence time of  $\text{NH}_4^+$ . We calculate that in summer, the in situ  $\text{NH}_4^+$  pool would be depleted in 2 to 27 days (median of 5 days) without coincident  $\text{NH}_4^+$  production. In addition, the net decline in  $\text{NH}_4^+$  concentration of  $0.31 \pm 0.97 \mu\text{M}$  between late summer and winter requires an average  $\text{NH}_4^+$  production rate of  $52.8 \pm 25.0 \text{ nM/day}$  given the observed  $\text{NH}_4^+$  assimilation rates. This estimate is remarkably similar to the only measurements of  $\text{NH}_4^+$  regeneration available for the Southern Ocean, measured near the Antarctic Peninsula in summer (average of  $55 \text{ nM day}^{-1}$ ; Goeyens et al., 1991).

By early spring, the  $\text{NH}_4^+$  concentrations had declined (Fig. 8d), implicating increased photosynthetic activity, and thus nutrient assimilation, following the alleviation of light-limitation. We suggest that any  $\text{NH}_4^+$  remaining in late winter would have been consumed in early spring prior to significant  $\text{NO}_3^-$  drawdown because far less energy (i.e., light) is required for its assimilation (Dortch, 1990). The high  $\text{NH}_4^+$  concentrations subsequently observed in late spring (mainly in the PFZ; Fig. 8e) can be explained by elevated heterotrophic activity in response to high levels of regional phytoplankton growth driven by frontal upwelling of limiting nutrients (Becquevort et al., 2000; Mayzaud et al., 2002).

From our six transects of surface  $\text{NH}_4^+$  concentrations across the Southern Ocean, we propose a seasonal cycle for mixed-layer  $\text{NH}_4^+$  south of the SAF (Fig. 8f). Our proposal is consistent with previous characterizations of the early summer-to-autumn evolution of Southern Ocean  $\text{NH}_4^+$  concentrations (i.e., from below detection due to phytoplankton assimilation to elevated due to net heterotrophy). However, it contradicts the hypothesis that  $\text{NH}_4^+$  will subsequently decline due to persistent but low rates of photosynthesis that yield insufficient biomass to support elevated heterotrophy in autumn, thus driving a coincident decrease in photosynthetic and heterotrophic activity (Koike et al., 1986; Serebrennikova & Fanning, 2004). Instead, our data evince a gradual decline in mixed-layer  $\text{NH}_4^+$  concentrations from late summer through winter. This decline can be explained by heterotrophic  $\text{NH}_4^+$  production outpacing  $\text{NH}_4^+$  removal in late summer/autumn, with  $\text{NH}_4^+$  regeneration then decreasing during winter to lower rates than the combined rate of  $\text{NH}_4^+$  assimilation and oxidation. By late spring,  $\text{NH}_4^+$  reaches concentrations similar to those observed in early summer as the improved growing conditions (i.e., elevated light and iron availability; Ellwood et al., 2008; Mtshali et al., 2019) allow phytoplankton to rapidly consume any  $\text{NH}_4^+$  remaining at the end of winter and subsequently produced in spring. An exception to this scenario is elevated, localized  $\text{NH}_4^+$  production near fronts, such as we observed in late spring 2019, which likely resulted from biological activity supported by frontal upwelling of silicate- and iron-bearing Upper Circumpolar Deep Water (Prézelin et al., 2000).

## 6. Summary and implications

Our study of the upper Southern Ocean, focused on the infrequently-sampled winter season, provides new insights into the internal cycling of N in the mixed layer of a globally-important

872 region. We attribute the elevated  $\text{NH}_4^+$  concentrations that persist in the winter mixed layer south  
 873 of the SAF to sustained heterotrophic  $\text{NH}_4^+$  production in excess of  $\text{NH}_4^+$  removal, driven by  
 874 temperature-, light-, and possibly iron-limitation of phytoplankton and nitrifiers. We further  
 875 suggest that heterotrophic bacteria are the main  $\text{NH}_4^+$  producers in winter and that the  
 876 contribution of external sources to the Southern Ocean's mixed-layer  $\text{NH}_4^+$  pool is negligible.  
 877 From observations of surface  $\text{NH}_4^+$  concentrations made between December 2018 and November  
 878 2019, we deduce that the elevated mixed-layer  $\text{NH}_4^+$  concentrations measured in winter cannot  
 879 be due solely to wintertime  $\text{NH}_4^+$  production. Instead, we propose that  $\text{NH}_4^+$  accumulates to its  
 880 highest concentrations in late summer following the peak phytoplankton growing season, after  
 881 which sustained heterotrophy throughout the autumn and winter prevents this  $\text{NH}_4^+$  from being  
 882 fully depleted until the early spring, even though the rate of  $\text{NH}_4^+$  removal must exceed that of  
 883  $\text{NH}_4^+$  production over this period. Measurements of heterotrophic  $\text{NH}_4^+$  production rates are  
 884 required to confirm the hypothesized seasonal cycle of  $\text{NH}_4^+$  in the Southern Ocean mixed layer,  
 885 and higher spatial resolution sampling of plankton community composition and N removal rates  
 886 may help to explain local variability in  $\text{NH}_4^+$  concentrations, particularly near the fronts.

887 In net, the Southern Ocean mixed layer is a biological source of  $\text{CO}_2$  to the atmosphere in autumn  
 888 and winter (Mongwe et al., 2018). The persistence of elevated  $\text{NH}_4^+$  concentrations across the  
 889 polar Southern Ocean between late summer and winter implies that this biological  $\text{CO}_2$   
 890 production occurs not only because  $\text{NO}_3^-$  drawdown is weak relative to  $\text{NO}_3^-$  supply at this time  
 891 (e.g., Gibson & Trull, 1999; Gray et al., 2018; Hauck et al., 2015; Mongwe et al., 2018; Shadwick  
 892 et al., 2015), but also because the ambient conditions allow for  $\text{NH}_4^+$  accumulation. There are  
 893 additional implications of our observations. For example,  $\text{NH}_4^+$  concentrations  $>1 \mu\text{M}$  (and at  
 894 times  $>0.5 \mu\text{M}$ ) have been reported to inhibit  $\text{NO}_3^-$  assimilation, including in the Southern Ocean  
 895 (Cochlan, 1986; Goeyens et al., 1995; Philibert et al., 2015; Reay et al., 2001). Inhibition of  $\text{NO}_3^-$   
 896 assimilation due to the seasonal accumulation of  $\text{NH}_4^+$  would constitute an inefficiency in the  
 897 biological pump. However, we observed little evidence of this effect in winter 2017 – the  
 898 southward decrease in  $\text{pNO}_3^-$  was not stronger than that of  $\text{pNH}_4^+$  despite the latitudinal increase  
 899 in  $\text{NH}_4^+$  concentration, and we observed no relationship between  $\text{NH}_4^+$  concentration and the  
 900 proportion of  $\text{NO}_3^-$  to  $\text{NO}_3^- + \text{NH}_4^+$  uptake (i.e., the f-ratio; Table S1).

901 The implications of  $\text{NH}_4^+$  cycling extend beyond the upper ocean to the atmosphere, since  
 902 ammonium aerosols that influence Earth's albedo (Tevlin & Murphy, 2019) are formed in the  
 903 marine boundary layer from reactions of  $\text{NH}_3$  gas with acidic species. In the remote Southern  
 904 Ocean, marine  $\text{NH}_3$  emissions, which are the largest natural contributors to  $\text{NH}_3$  globally, are  
 905 likely the dominant local source of  $\text{NH}_3$  to the atmosphere (Paulot et al., 2015). Surface ocean  
 906  $\text{NH}_4^+$  concentrations play a central role in determining the sign and magnitude of the air-sea  $\text{NH}_3$   
 907 flux, along with wind speed, surface ocean temperature, and pH. Therefore, the biogeochemical  
 908 pathways that underpin seasonal changes in surface ocean  $\text{NH}_4^+$  concentrations represent an  
 909 important control on the remote Southern Ocean air-sea  $\text{NH}_3$  flux, with consequences for aerosol  
 910 composition, cloud formation, and climate (Altieri et al., 2021).

Deleted: the

Deleted: mixed layer is a

Deleted: source of

Deleted: to the atmosphere for half the year,

## Acknowledgements

We are grateful to Captain Knowledge Bengu and the crew of the R/V *SA Agulhas II*, and Chief Scientists Hermann Luyt, Marcello Vichi, and Thomas Ryan-Keogh. We thank Tahlia Henry for CTD operations and CTD and SDS data processing. We are grateful to the students from the Cape Peninsula University of Technology for help with sample collection and analysis of chl-a, and thank Raquel Flynn, Mishka Rawatlal, and Raymond Roman for assistance with nutrient analyses. We acknowledge the Flow Cytometry Core Facility at the University of Cape Town (UCT) and the efforts of Ian Newton at the Stable Light Isotope Laboratory (UCT). This work was supported by the South African Departments of Forestry, Fisheries, and Environment (formerly Environmental Affairs) and Science and Innovation (DSI), and the National Research Foundation (NRF) through the South African National Antarctic Program (SANAP; 110732 to K.E.A and 105539, 110735, and 129232 to S.E.F.), Equipment-related Travel and Training Grant (118615 to K.E.A.), Competitive Support for Rated Researchers Grant (111716 to K.E.A.), and Incentive Fund (115335 to S.E.F.). S.S., M.M., K.A.M.S., and J.M.B. acknowledge funding from the NRF through postgraduate scholarships (120105, 112380, 113193, and 108757). S.S. was partially supported by a UCT Vice-Chancellor Research Scholarship and M.M. by the UCT Harry Crossley Foundation Research Fellowship. S.E.F. and K.E.A. acknowledge the support of the UCT Vice-Chancellor Future Leaders 2030 programme. S.E.F. acknowledges an African Academy of Sciences/Royal Society FLAIR fellowship and K.E.A. acknowledges support from UCT through a University Research Council Launching Grant and a University Equipment Committee Grant. We further acknowledge the support of the DSI Biogeochemistry Research Infrastructure Platform (BIOGRIP).

## 7. References

- Aarnos, H., Ylöstalo, P. and Vähätalo, A.V., (2012). Seasonal phototransformation of dissolved organic matter to ammonium, dissolved inorganic carbon, and labile substrates supporting bacterial biomass across the Baltic Sea. *Journal of Geophysical Research: Biogeosciences*, 117(G1).
- Allredge, A.L. and Gotschalk, C., (1988). In situ settling behavior of marine snow 1. *Limnology and Oceanography*, 33(3), pp.339-351.
- Altabet, M.A., (1988). Variations in nitrogen isotopic composition between sinking and suspended particles: Implications for nitrogen cycling and particle transformation in the open ocean. *Deep Sea Research Part A. Oceanographic Research Papers*, 35(4), pp.535-554.
- Altieri, K.E., Spence, K.A.M., and Smith, S. (2021). Air-Sea Ammonia Fluxes Calculated from High-Resolution Summertime Observations Across the Atlantic Southern Ocean. *Geophysical Research Letters*.
- Amin, S.A., Moffett, J.W., Martens-Habben, W., Jacquot, J.E., Han, Y., Devol, A., Ingalls, A.E., Stahl, D.A. and Armbrust, E.V., (2013). Copper requirements of the ammonia-oxidizing archaeon *Nitrosopumilus maritimus* SCM1 and implications for nitrification in the marine environment. *Limnology and Oceanography*, 58(6), pp.2037-2045.
- Armstrong, R.A., (1999). An optimization-based model of iron-light-ammonium colimitation of nitrate uptake and phytoplankton growth. *Limnology and Oceanography*, 44(6), pp.1436-1446.
- Arrigo, K. R., van Dijken, G. L., and Bushinsky, S. (2008). Primary production in the Southern Ocean, 1997–2006. *Journal of Geophysical Research*, 113(C8), C08004.
- Arteaga, L.A., Pahlow, M., Bushinsky, S.M. and Sarmiento, J.L., (2019). Nutrient controls on export production in the Southern Ocean. *Global Biogeochemical Cycles*, 33(8), pp.942-956.
- Atkinson, A., Ward, P., Hunt, B.P.V., Pakhomov, E.A. and Hosie, G.W., (2012). An overview of Southern Ocean zooplankton data: abundance, biomass, feeding and functional relationships. *CCLAMR Science*, 19, pp.171-218.
- Baer, S.E., Connelly, T.L., Sipler, R.E., Yager, P.L. and Bronk, D.A., (2014). Effect of temperature on rates of ammonium uptake and nitrification in the western coastal Arctic during winter, spring, and summer. *Global Biogeochemical Cycles*, 28(12), pp.1455-1466.
- Bagwell, J.E., (2009). Transcriptional Response of Nitrogen Uptake and Assimilation in Marine Diatoms; *Thalassiosira pseudonana* and *Thalassiosira weissflogii* (Doctoral dissertation, University of North Carolina Wilmington).

966 Baird, M.E., Emsley, S.M. and Mcglade, J.M., (2001). Modelling the interacting effects of nutrient uptake, light capture  
967 and temperature on phytoplankton growth. *Journal of Plankton Research*, 23(8), pp.829-840.

968 Bakker, D. C. E., Pfeil, B., Landa, C. S., Metzl, N., O'Brien, K. M., Olsen, A., et al. (2016). A multi-decade record of  
969 high-quality FCO<sub>2</sub> data in version 3 of the Surface Ocean CO<sub>2</sub> Atlas (SOCAT). *Earth System Science Data*, 8, 383–413.

970 Bathmann, U.V., Scharek, R., Klaas, C., Dubischar, C.D. and Smetacek, V., (1997). Spring development of phytoplankton  
971 biomass and composition in major water masses of the Atlantic sector of the Southern Ocean. *Deep Sea Research Part II:*  
972 *Topical Studies in Oceanography*, 44(1-2), pp.51-67.

973 Becquevort, S., Menon, P., and Lancelot, C. (2000). Differences of the protozoan biomass and grazing during spring and  
974 summer in the Indian sector of the Southern Ocean. *Polar Biology*, 23(5), 309–320.

975 Belkin, I. M., and Gordon, A. L. (1996). Southern Ocean fronts from the Greenwich meridian to Tasmania. *Journal of*  
976 *Geophysical Research C: Oceans*, 101(C2), 3675–3696.

977 Bendschneider, K. and Robinson, R.J., (1952). A new spectrophotometric method for the determination of nitrite in sea  
978 water.

979 Bianchi, M., Feliatra, F., Tréguer, P., Vincendeau, M.A. and Morvan, J., (1997). Nitrification rates, ammonium and nitrate  
980 distribution in upper layers of the water column and in sediments of the Indian sector of the Southern Ocean. *Deep Sea*  
981 *Research Part II: Topical Studies in Oceanography*, 44(5), pp.1017-1032.

982 Billen, G., (1984). Heterotrophic utilization and regeneration of nitrogen. In *Heterotrophic activity in the sea*. NATO  
983 Conference Series (IV Marine Sciences), vol 15. Springer, Boston, MA.

984 Bouwman, A. F., Lee, D. S., Asman, W. A. H., Dentener, F. J., Van Der Hoek, K. W., and Olivier, J. G. J. (1997). A  
985 global high-resolution emission inventory for ammonia. *Global Biogeochemical Cycles*, 11(4), 561–587.

986 Boyd, P.W., Crossley, A.C., DiTullio, G.R., Griffiths, F.B., Hutchins, D.A., Queguiner, B., Sedwick, P.N. and Trull,  
987 T.W., (2001). Control of phytoplankton growth by iron supply and irradiance in the subantarctic Southern Ocean:  
988 Experimental results from the SAZ Project. *Journal of Geophysical Research: Oceans*, 106(C12), pp.31573-31583.

989 Boyd, P. W., Rynearson, T. A., Armstrong, E. A., Fu, F., Hayashi, K., Hu, Z., Hutchins, D. A., Kudela, R. M., Litchman,  
990 E., Mulholland, M. R., Passow, U., Strzpek, R. F., Whittaker, K. A., Yu, E., and Thomas, M. K. (2013). Marine  
991 Phytoplankton Temperature versus Growth Responses from Polar to Tropical Waters - Outcome of a Scientific  
992 Community-Wide Study. *PLoS ONE*, 8(5), 1–17.

993 Bracher, A. U., Kroon, B. M. A., and Lucas, M. I. (1999). Primary production, physiological state and composition of  
994 phytoplankton in the Atlantic sector of the Southern Ocean. *Marine Ecology Progress Series*, 190, 1–16.

995 Brightman, R.I. and Smith Jr, W.O., (1989). Photosynthesis-irradiance relationships of Antarctic phytoplankton during  
996 austral winter. *Marine Ecology Progress Series*, pp.143-151.

997 Broecker, W.S. and Peng, T.H., (1992). Interhemispheric transport of carbon dioxide by ocean circulation. *Nature*,  
998 356(6370), pp.587-589.

999 Brzezinski, M. A. (1988). Vertical distribution of ammonium in stratified oligotrophic waters. *Limnol. Oceanogr.* 33(5),  
1000 1176–1182.

1001 Buongiorno Nardelli, B., Guinehut, S., Verbrugge, N., Cotroneo, Y., Zambianchi, E. and Iudicone, D., (2017). Southern  
1002 Ocean mixed-layer seasonal and interannual variations from combined satellite and in situ data. *Journal of Geophysical*  
1003 *Research: Oceans*, 122(12), pp.10042-10060.

1004 Campitelli E. (2019). metR: Tools for Easier Analysis of Meteorological Fields. R package version 0.5.0.  
1005 <https://CRAN.R-project.org/package=metR>

1006 Capone, D.G., Bronk, D.A., Mulholland, M.R. and Carpenter, E.J. eds., (2008). *Nitrogen in the marine environment*.  
1007 Elsevier.

1008 Carvalho, F., Kohut, J., Oliver, M.J. and Schofield, O., (2017). Defining the ecologically relevant mixed-layer depth for  
1009 Antarctica's coastal seas. *Geophysical Research Letters*, 44(1), pp.338-345.

1010 Casey, J.R., Lomas, M.W., Michelou, V.K., Dyhrman, S.T., Orchard, E.D., Ammerman, J.W. and Sylvan, J.B., (2009).  
1011 Phytoplankton taxon-specific orthophosphate (Pi) and ATP utilization in the western subtropical North Atlantic. *Aquatic*  
1012 *microbial ecology*, 58(1), pp.31-44.

1013 Cavagna, A.J., Fripiat, F., Elskens, M., Mangion, P., Chirurgien, L., Closset, I., Lasbleiz, M., Florez-Leiva, L., Cardinal,  
1014 D., Leblanc, K., and Fernandez, C., (2015). Production regime and associated N cycling in the vicinity of Kerguelen  
1015 Island, Southern Ocean. *Biogeosciences*, 12(21), pp.6515-6528.

1016 Cavaleri, D.J. and Parkinson, C.L., (2008). Antarctic sea ice variability and trends, 1979–2006. *Journal of Geophysical*  
1017 *Research: Oceans*, 113(C7).

1018 Cavender-Bares, K.K., Mann, E.L., Chisholm, S.W., Ondrusek, M.E. and Bidigare, R.R., (1999). Differential response of  
1019 equatorial Pacific phytoplankton to iron fertilization. *Limnology and Oceanography*, 44(2), pp.237-246.

1020 Checkley Jr, D.M. and Miller, C.A., (1989). Nitrogen isotope fractionation by oceanic zooplankton. *Deep Sea Research*  
1021 *Part A. Oceanographic Research Papers*, 36(10), pp.1449-1456.

- Chisholm, S. W. (1992). Phytoplankton Size. In *Primary Productivity and Biogeochemical Cycles in the Sea* (pp. 213–237). Springer US.
- Church, M.J., DeLong, E.F., Ducklow, H.W., Karner, M.B., Preston, C.M. and Karl, D.M., (2003). Abundance and distribution of planktonic Archaea and Bacteria in the waters west of the Antarctic Peninsula. *Limnology and Oceanography*, 48(5), pp.1893-1902.
- Coale, K. H., Gordon, R. M., and Wang, X. (2005). The distribution and behaviour of dissolved and particulate iron and zinc in the Ross Sea and Antarctic circumpolar current along 170°W. *Deep-Sea Research Part I: Oceanographic Research Papers*, 52(2), 295–318.
- Cochlan, W.P., (1986). Seasonal study of uptake and regeneration of nitrogen on the Scotian Shelf. *Continental Shelf Research*, 5(5), pp.555-577.
- Cochlan, W.P., (2008). Nitrogen uptake in the Southern Ocean. *Nitrogen in the Marine Environment*, edited by: Capone, DG, Bronk, DA, Mulholland, MR, and Carpenter, EJ, 2nd Edition, Academic Press, Elsevier, pp.569-596.
- Cochlan, W.P., Bronk, D.A. and Coale, K.H., (2002). Trace metals and nitrogenous nutrition of Antarctic phytoplankton: experimental observations in the Ross Sea. *Deep Sea Research Part II: Topical Studies in Oceanography*, 49(16), pp.3365-3390.
- Coello-Camba, A. and Agustí, S., (2017). Thermal thresholds of phytoplankton growth in polar waters and their consequences for a warming polar ocean. *Frontiers in Marine Science*, 4, p.168.
- Cota, G.F., Smith, W.O., Nelson, D.M., Muench, R.D. and Gordon, L.I., (1992). Nutrient and biogenic particulate distributions, primary productivity and nitrogen uptake in the Weddell-Scotia Sea marginal ice zone during winter. *Journal of Marine Research*, 50(1), pp.155-181
- Daly, K. L., Smith, W. O., Johnson, G. C., DiTullio, G. R., Jones, D. R., Mordy, C. W., Feely, R. A., Hansell, D. A., and Zhang, J.-Z. (2001). Hydrography, nutrients, and carbon pools in the Pacific sector of the Southern Ocean: Implications for carbon flux. *Journal of Geophysical Research: Oceans*, 106(C4), 7107–7124.
- Deary, A. (2020). A high-resolution study of the early- to late summer progression in primary production and carbon export potential in the Atlantic Southern Ocean. (Honours thesis, University of Cape Town).
- del Giorgio, P.A. and Cole, J.J., (1998). Bacterial growth efficiency in natural aquatic systems. *Annual Review of Ecology and Systematics*, 29(1), pp.503-541.
- Dennett, M. R., Mathot, S., Caron, D. A., Smith, W. O., and Lonsdale, D. J. (2001). Abundance and distribution of phototrophic and heterotrophic nano- and microplankton in the southern Ross Sea. *Deep-Sea Research Part II: Topical Studies in Oceanography*, 48(19–20), 4019–4037.
- Deppeler, S.L. and Davidson, A.T., (2017). Southern Ocean phytoplankton in a changing climate. *Frontiers in Marine Science*, 4, p.40.
- Detmer, A.E. and Bathmann, U.V., (1997). Distribution patterns of autotrophic pico- and nanoplankton and their relative contribution to algal biomass during spring in the Atlantic sector of the Southern Ocean. *Deep Sea Research Part II: Topical Studies in Oceanography*, 44(1-2), pp.299-320.
- DiFiore, P. J., Sigman, D. M., Trull, T. W., Lourey, M. J., Karsh, K., Cane, G., and Ho, R. (2006). Nitrogen isotope constraints on subantarctic biogeochemistry. *Journal of Geophysical Research: Oceans*, 111(8).
- Dixon, G.K. and Syrett, P.J., (1988). The growth of dinoflagellates in laboratory cultures. *New phytologist*, 109(3), pp.297-302.
- Doney, S.C., Mahowald, N., Lima, I., Feely, R.A., Mackenzie, F.T., Lamarque, J.F. and Rasch, P.J., (2007). Impact of anthropogenic atmospheric nitrogen and sulfur deposition on ocean acidification and the inorganic carbon system. *Proceedings of the National Academy of Sciences*, 104(37), pp.14580-14585.
- Dong, S., Sprintall, J., Gille, S.T. and Talley, L., (2008). Southern Ocean mixed-layer depth from Argo float profiles. *Journal of Geophysical Research: Oceans*, 113(C6).
- Dortch, Q. (1990). The interaction between ammonium and nitrate uptake in phytoplankton. *Marine Ecology Progress Series*, 61(1), 183–201.
- Dugdale, R. C., and Goering, J. J. (1967). Uptake of new and regenerated forms of nitrogen in primary productivity. *Limnology and Oceanography*, 12(2), 196–206.
- Dugdale, R.C. and Wilkerson, F.P., (1986). The use of <sup>15</sup>N to measure nitrogen uptake in eutrophic oceans; experimental considerations 1, 2. *Limnology and Oceanography*, 31(4), pp.673-689.
- Ellwood, M.J., Boyd, P.W. and Sutton, P., (2008). Winter-time dissolved iron and nutrient distributions in the Subantarctic Zone from 40–52S; 155–160E. *Geophysical Research Letters*, 35(11).
- El-Sayed, S., (1984). Productivity of the Antarctic waters—a reappraisal. In *Marine phytoplankton and productivity* (pp. 19-34). Springer, Berlin, Heidelberg.
- Eppley, R.W. and Peterson, B.J., (1979). Particulate organic matter flux and planktonic new production in the deep ocean. *Nature*, 282(5740), pp.677-680.



Fan, C., Glibert, P.M., and Burkholder, J.M., (2003). Characterization of the affinity for nitrogen, uptake kinetics, and environmental relationships for *Prorocentrum minimum* in natural blooms and laboratory cultures. *Harmful Algae*, 2(4), pp.283-299.

Fawcett, S. E., and Ward, B. B. (2011). Phytoplankton succession and nitrogen utilization during the development of an upwelling bloom. *Marine Ecology Progress Series*, 428, 13–31.

Fawcett, S.E., Lomas, M.W., Casey, J.R., Ward, B.B. and Sigman, D.M., (2011). Assimilation of upwelled nitrate by small eukaryotes in the Sargasso Sea. *Nature Geoscience*, 4(10), pp.717-722.

Fawcett, S.E., Lomas, M.W., Ward, B.B. and Sigman, D.M., (2014). The counterintuitive effect of summer-to-fall mixed layer deepening on eukaryotic new production in the Sargasso Sea. *Global biogeochemical cycles*, 28(2), pp.86-102.

Fiala, M. and Oriol, L., (1990). Light-temperature interactions on the growth of Antarctic diatoms. *Polar Biology*, 10(8), pp.629-636.

Fiala, M., Semeneh, M. and Oriol, L., (1998). Size-fractionated phytoplankton biomass and species composition in the Indian sector of the Southern Ocean during austral summer. *Journal of Marine Systems*, 17(1-4), pp.179-194.

Finkel, Z.V., Irwin, A.J. and Schofield, O., (2004). Resource limitation alters the 3/4 size scaling of metabolic rates in phytoplankton. *Marine Ecology Progress Series*, 273, pp.269-279.

Finley A., Banerjee S., and Hjelte Ø. (2017). MBA: Multilevel B-Spline Approximation. package version 0.0-9. <https://CRAN.R-project.org/package=MBA>

Forsythe, W.C., Rykiel Jr, E.J., Stahl, R.S., Wu, H.I. and Schoolfield, R.M., (1995). A model comparison for daylength as a function of latitude and day of year. *Ecological Modelling*, 80(1), pp.87-95.

Flynn, R.F., Burger, J.M., Pillay, K. and Fawcett, S.E., (2018). Wintertime rates of net primary production and nitrate and ammonium uptake in the southern Benguela upwelling system. *African Journal of Marine Science*, 40(3), pp.253-266.

Franck, V.M., Smith, G.J., Bruland, K.W. and Brzezinski, M.A., (2005). Comparison of size-dependent carbon, nitrate, and silicic acid uptake rates in high-and low-iron waters. *Limnology and Oceanography*, 50(3), pp.825-838.

Francois, R., Altabet, M.A. and Burckle, L.H., (1992). Glacial to interglacial changes in surface nitrate utilization in the Indian sector of the Southern Ocean as recorded by sediment  $\delta^{15}\text{N}$ . *Paleoceanography*, 7(5), pp.589-606.

Fransson, A., Chierici, M., Anderson, L. and David, R., (2004). Transformation of carbon and oxygen in the surface layer of the eastern Atlantic sector of the Southern Ocean. *Deep Sea Research Part II: Topical Studies in Oceanography*, 51(22-24), pp.2757-2772.

Frigstad, H., Andersen, T., Hessen, D.O., Naustvoll, L.J., Johnsen, T.M. and Bellerby, R.G., (2011). Seasonal variation in marine C: N: P stoichiometry: can the composition of seston explain stable Redfield ratios?. *Biogeosciences*, 8(10), pp.2917-2933.

Fripiat, F., Elskens, M., Trull, T.W., Blain, S., Cavagna, A.J., Fernandez, C., Fonseca-Batista, D., Planchon, F., Raimbault, P., Roukaerts, A. and Dehairs, F., (2015). Significant mixed layer nitrification in a natural iron-fertilized bloom of the Southern Ocean. *Global Biogeochemical Cycles*, 29(11), pp.1929-1943.

Fripiat, F., Martínez-García, A., Fawcett, S.E., Kemeny, P.C., Studer, A.S., Smart, S.M., Rubach, F., Oleynik, S., Sigman, D.M. and Haug, G.H., (2019). The isotope effect of nitrate assimilation in the Antarctic Zone: Improved estimates and paleoceanographic implications. *Geochimica et Cosmochimica Acta*, 247, pp.261-279.

Fripiat, F., Martínez-García, A., Marconi, D., Fawcett, S.E., Kopf, S., Luu, V., Rafter, P., Zhang, R., Sigman, D., and Haug, G., (2021). Nitrogen isotopic constraints on nutrient transport to the upper ocean. *Nature Geoscience*.

Frölicher, T.L., Sarmiento, J.L., Paynter, D.J., Dunne, J.P., Krasting, J.P., and Winton, M., (2015). Dominance of the Southern Ocean in anthropogenic carbon and heat uptake in CMIP5 models. *Journal of Climate*, 28(2), pp.862-886.

Froneman, P.W., Anson, I.J., Pakhomov, E.A. and Lutjeharms, J.R.E., (1999). Plankton community structure in the physical environment surrounding the Prince Edward Islands (Southern Ocean). *Polar Biology*, 22(3), pp.145-155.

Fujiki, T. and Taguchi, S., (2002). Variability in chlorophyll a specific absorption coefficient in marine phytoplankton as a function of cell size and irradiance. *Journal of Plankton Research*, 24(9), pp.859-874.

Gao, Y., Kaufman, Y. J., Tanré, D., Kolber, D., and Falkowski, P. G. (2001). Seasonal distributions of aeolian iron fluxes to the global ocean. *Geophysical Research Letters*, 28(1), pp.29–32.

Gasol, J.M. and del Giorgio, P.A., (2000). Using flow cytometry for counting natural planktonic bacteria and understanding the structure of planktonic bacterial communities. *Scientia Marina*, 64(2), pp.197-224.

Gibson, J.A. and Trull, T.W., (1999). Annual cycle of  $\text{fCO}_2$  under sea-ice and in open water in Prydz Bay, East Antarctica. *Marine Chemistry*, 66(3-4), pp.187-200.

Glibert, P.M., (1982). Regional studies of daily, seasonal and size fraction variability in ammonium remineralization. *Marine Biology*, 70(2), pp.209-222.

Goericke, R., (1998). Response of phytoplankton community structure and taxon-specific growth rates to seasonally varying physical forcing in the Sargasso Sea off Bermuda. *Limnology and Oceanography*, 43(5), pp.921-935.

1133 Goeyens, L., Tréguer, P., Lancelot, C., Mathot, S., Becquevort, S., Morvan, J., Dehairs, F. and Baeyens, W., (1991).  
1134 Ammonium regeneration in the Scotia-Weddell Confluence area during spring 1988. *Marine Ecology Progress Series*,  
1135 pp.241-252.

1136 Goeyens, L., Tréguer, P., Baumann, M. E. M., Baeyens, W., and Dehairs, F. (1995). The leading role of ammonium in the  
1137 nitrogen uptake regime of Southern Ocean marginal ice zones. *Journal of Marine Systems*, 6(4), pp.345–361.

1138 Granger, J., Sigman, D.M., Needoba, J.A. and Harrison, P.J., (2004). Coupled nitrogen and oxygen isotope fractionation  
1139 of nitrate during assimilation by cultures of marine phytoplankton. *Limnology and Oceanography*, 49(5), pp.1763-1773.

1140 Granger, J., Sigman, D.M., Rohde, M.M., Maldonado, M.T. and Tortell, P.D., (2010). N and O isotope effects during  
1141 nitrate assimilation by unicellular prokaryotic and eukaryotic plankton cultures. *Geochimica et Cosmochimica Acta*, 74(3),  
1142 pp.1030-1040.

1143 Gray, A.R., Johnson, K.S., Bushinsky, S.M., Riser, S.C., Russell, J.L., Talley, L.D., Wanninkhof, R., Williams, N.L. and  
1144 Sarmiento, J.L., (2018). Autonomous biogeochemical floats detect significant carbon dioxide outgassing in the high-  
1145 latitude Southern Ocean. *Geophysical Research Letters*, 45(17), pp.9049-9057.

1146 Greene, R.M., Geider, R.J. and Falkowski, P.G., (1991). Effect of iron limitation on photosynthesis in a marine diatom.  
1147 *Limnology and Oceanography*, 36(8), pp.1772-1782.

1148 Harrison, W.G., (1976). Nitrate metabolism of the red tide dinoflagellate *Gonyaulax polyedra* Stein. *Journal of*  
1149 *Experimental Marine Biology and Ecology*, 21(3), pp.199-209.

1150 Hasle, R.G., (1978). The inverted microscope method. *Phytoplankton manual*, pp.88-96.

1151 Hauck, J., Völker, C., Wolf-Gladrow, D.A., Laufkötter, C., Vogt, M., Aumont, O., Bopp, L., Buitenhuis, E.T., Doney,  
1152 S.C., Dunne, J. and Gruber, N., (2015). On the Southern Ocean CO<sub>2</sub> uptake and the role of the biological carbon pump in  
1153 the 21st century. *Global Biogeochemical Cycles*, 29(9), pp.1451-1470.

1154 Henley, S.F., Tuerena, R.E., Annett, A.L., Fallick, A.E., Meredith, M.P., Venables, H.J., Clarke, A. and Ganeshram, R.S.,  
1155 (2017). Macronutrient supply, uptake and recycling in the coastal ocean of the west Antarctic Peninsula. *Deep Sea*  
1156 *Research Part II: Topical Studies in Oceanography*, 139, pp.58-76.

1157 Henley, S.F., Cavan, E.L., Fawcett, S.E., Kerr, R., Monteiro, T., Sherrell, R.M., Bowie, A.R., Boyd, P.W., Barnes, D.K.,  
1158 Schloss, I.R., Marshall, T., Flynn, R., and Smith, S., (2020). Changing biogeochemistry of the Southern Ocean and its  
1159 ecosystem implications. *Frontiers in Marine Science*, 7, p.581.

1160 Hense, I., Bathmann, U.V. and Timmermann, R., (2000). Plankton dynamics in frontal systems of the Southern  
1161 Ocean. *Journal of Marine Systems*, 27(1-3), pp.235-252.

1162 Herbert, R.A., (1999). Nitrogen cycling in coastal marine ecosystems. *FEMS microbiology reviews*, 23(5), pp.563-590.

1163 Hewes, C.D., Holm-Hansen, O. and Sakshaug, E., (1985). Alternate carbon pathways at lower trophic levels in the  
1164 Antarctic food web. *Antarctic nutrient cycles and food webs*. pp. 277-28.

1165 Hewes, C.D., Sakshaug, E., Reid, F.M., and Holm-Hansen, O., (1990). Microbial autotrophic and heterotrophic eucaryotes  
1166 in Antarctic waters: relationships between biomass and chlorophyll, adenosine triphosphate and particulate organic  
1167 carbon. *Marine Ecology Progress Series*, pp.27-35.

1168 Hiscock, M.R., Marra, J., Smith Jr, W.O., Goericke, R., Measures, C., Vink, S., Olson, R.J., Sosik, H.M. and Barber, R.T.,  
1169 (2003). Primary productivity and its regulation in the Pacific Sector of the Southern Ocean. *Deep Sea Research Part II:*  
1170 *Topical Studies in Oceanography*, 50(3-4), pp.533-558.

1171 Holm-Hansen, O., Mitchell, B.G., Hewes, C.D. and Karl, D.M., (1989). Phytoplankton blooms in the vicinity of Palmer  
1172 Station, Antarctica. *Polar Biology*, 10(1), pp.49-57.

1173 Holmes, R.M., Aminot, A., Kérouel, R., Hooker, B.A. and Peterson, B.J., (1999). A simple and precise method for  
1174 measuring ammonium in marine and freshwater ecosystems. *Canadian Journal of Fisheries and Aquatic Sciences*, 56(10),  
1175 pp.1801-1808.

1176 Holzer, M., Primeau, F.W., DeVries, T. and Matear, R., (2014). The Southern Ocean silicon trap: Data-constrained  
1177 estimates of regenerated silicic acid, trapping efficiencies, and global transport paths. *Journal of Geophysical Research:*  
1178 *Oceans*, 119(1), pp.313-331.

1179 Honjo, S., Francois, R., Manganini, S., Dymond, J. and Collier, R., (2000). Particle fluxes to the interior of the Southern  
1180 Ocean in the Western Pacific sector along 170 W. *Deep Sea Research Part II: Topical Studies in Oceanography*, 47(15-  
1181 16), pp.3521-3548.

1182 Hooper, A.B. and Terry, K.R., (1974). Photoinactivation of ammonia oxidation in *Nitrosomonas*. *Journal of Bacteriology*,  
1183 119(3), pp.899-906.

1184 Horak, R.E., Qin, W., Schauer, A.J., Armbrust, E.V., Ingalls, A.E., Moffett, J.W., Stahl, D.A. and Devol, A.H., (2013).  
1185 Ammonia oxidation kinetics and temperature sensitivity of a natural marine community dominated by Archaea. *The ISME*  
1186 *journal*, 7(10), pp.2023-2033.

1187 Horrigan, S. G., & Springer, A. L. (1990). Oceanic and estuarine ammonium oxidation: Effects of light. *Limnology and*  
1188 *Oceanography*, 35(2), pp.479–482.

- Huang, K., Feng, Q., Zhang, Y., Ou, L., Cen, J., Lu, S. and Qi, Y., (2020). Comparative uptake and assimilation of nitrate, ammonium, and urea by dinoflagellate *Karenia mikimotoi* and diatom *Skeletonema costatum* sl in the coastal waters of the East China Sea. *Marine Pollution Bulletin*, 155, p.11200.
- Hudson, R.J. and Morel, F.M., (1993). Trace metal transport by marine microorganisms: implications of metal coordination kinetics. *Deep Sea Research Part I: Oceanographic Research Papers*, 40(1), pp.129-150.
- Hutchins, D.A., Sedwick, P.N., DiTullio, G.R., Boyd, P.W., Queguiner, B., Griffiths, F.B. and Crossley, C., (2001). Control of phytoplankton growth by iron and silicic acid availability in the subantarctic Southern Ocean: Experimental results from the SAZ Project. *Journal of Geophysical Research: Oceans*, 106(C12), pp.31559-31572.
- Iida, T. and Odate, T., (2014). Seasonal variability of phytoplankton biomass and composition in the major water masses of the Indian Ocean sector of the Southern Ocean. *Polar Science*, 8(3), pp.283-297.
- Ishikawa, A., Wright, S.W., van den Enden, R., Davidson, A.T. and Marchant, H.J., (2002). Abundance, size structure and community composition of phytoplankton in the Southern Ocean in the austral summer 1999/2000. *Polar Biosciences*, 15, pp.11-26.
- Jacobson, D. M., and Anderson, D. M. (1996). Widespread phagocytosis of ciliates and other protists by marine mixotrophic and heterotrophic thecate dinoflagellates. *Journal of Phycology*, 32(2), 279–285.
- Janssen, D.J., Sieber, M., Ellwood, M.J., Conway, T.M., Barrett, P.M., Chen, X., de Souza, G.F., Hassler, C.S. and Jaccard, S.L., (2020). Trace metal and nutrient dynamics across broad biogeochemical gradients in the Indian and Pacific sectors of the Southern Ocean. *Marine chemistry*, 221, p.103773.
- Jeong, H.J. and Latz, M.I., (1994). Growth and grazing rates of the heterotrophic dinoflagellates *Protoperidinium* spp. on red tide dinoflagellates. *Marine Ecology-Progress Series*, 106, pp.173-173.
- Jiang, H.B., Fu, F.X., Rivero-Calle, S., Levine, N.M., Sañudo-Wilhelmy, S.A., Qu, P.P., Wang, X.W., Pinedo-Gonzalez, P., Zhu, Z. and Hutchins, D.A., (2018). Ocean warming alleviates iron limitation of marine nitrogen fixation. *Nature Climate Change*, 8(8), pp.709-712.
- Johnson, K.S., Plant, J.N., Dunne, J.P., Talley, L.D. and Sarmiento, J.L., (2017). Annual nitrate drawdown observed by SOCCOM profiling floats and the relationship to annual net community production. *Journal of Geophysical Research: Oceans*, 122(8), pp.6668-6683.
- Jones, R.D., Morita, R.Y., Koops, H.P. and Watson, S.W., (1988). A new marine ammonium-oxidizing bacterium, *Nitrosomonas cryotolerans* sp. nov. *Canadian journal of microbiology*, 34(10), pp.1122-1128.
- Joubert, W. R., Thomalla, S. J., Waldron, H. N., Lucas, M. I., Boye, M., Le Moigne, F. A. C., Planchon, F., and Speich, S. (2011). Nitrogen uptake by phytoplankton in the Atlantic sector of the Southern Ocean during late austral summer. *Biogeosciences*, 8(10), pp.2947–2959.
- Kassambara A. (2019). ggpubr: 'ggplot2' Based Publication Ready Plots. R package version 0.2.4. <https://CRAN.R-project.org/package=ggpubr>
- Kattner, G., Thomas, D.N., Haas, C., Kennedy, H. and Dieckmann, G.S., (2004). Surface ice and gap layers in Antarctic sea ice: highly productive habitats. *Marine Ecology Progress Series*, 277, pp.1-12.
- Kemeny, P.C., Kast, E.R., Hain, M.P., Fawcett, S.E., Fripiat, F., Studer, A.S., Martínez-García, A., Haug, G.H. and Sigman, D.M., (2018). A seasonal model of nitrogen isotopes in the ice age Antarctic Zone: Support for weakening of the Southern Ocean upper overturning cell. *Paleoceanography and Paleoclimatology*, 33(12), pp.1453-1471.
- Kirchman, D. L. (1994). The Uptake of Inorganic Nutrients by Heterotrophic Bacteria. *Microbial Ecology* 28(2), pp.255–71.
- Kitzinger, K., Padilla, C.C., Marchant, H.K., Hach, P.F., Herbold, C.W., Kidane, A.T., Könneke, M., Littmann, S., Mooshammer, M., Niggemann, J. and Petrov, S., (2019). Cyanate and urea are substrates for nitrification by Thaumarchaeota in the marine environment. *Nature microbiology*, 4(2), pp.234-243.
- Klawonn, I., Bonaglia, S., Whitehouse, M.J., Littmann, S., Tienken, D., Kuypers, M.M., Brüchert, V. and Ploug, H., (2019). Untangling hidden nutrient dynamics: rapid ammonium cycling and single-cell ammonium assimilation in marine plankton communities. *The ISME journal*, 13(8), pp.1960-1974.
- Knapp, A.N., Dekaezemacker, J., Bonnet, S., Sohm, J.A. and Capone, D.G., (2012). Sensitivity of *Trichodesmium* erythraeum and *Crocosphaera watsonii* abundance and N<sub>2</sub> fixation rates to varying NO<sub>3</sub><sup>-</sup> and PO<sub>43</sub><sup>-</sup> concentrations in batch cultures. *Aquatic microbial ecology*, 66(3), pp.223-236.
- Kobayashi, F. and Takahashi, K., (2002). Distribution of diatoms along the equatorial transect in the western and central Pacific during the 1999 La Niña conditions. *Deep Sea Research Part II: Topical Studies in Oceanography*, 49(13-14), pp.2801-2821.
- Koike, I., Holm-Hansen, O., and Biggs, D. C. (1986). Phytoplankton With Special Reference To Ammonium Cycling. *Marine Ecology*, 30, pp.105–116.
- Kopczyńska, E. E., Savoye, N., Dehairs, F., Cardinal, D., and Elskens, M. (2007). Spring phytoplankton assemblages in the Southern Ocean between Australia and Antarctica. *Polar Biology*, 31(1), pp.77–88.

1245 Kottmeier, S.T. and Sullivan, C.W., (1987). Late winter primary production and bacterial production in sea ice and  
1246 seawater west of the Antarctic Peninsula. *Mar Ecol Prog Ser*, 36, pp.287-298.

1247 Krell, A., Schnack-Schiel, S.B., Thomas, D.N., Kattner, G., Zipan, W. and Dieckmann, G.S., (2005). Phytoplankton  
1248 dynamics in relation to hydrography, nutrients and zooplankton at the onset of sea ice formation in the eastern Weddell  
1249 Sea (Antarctica). *Polar Biology*, 28(9), pp.700-713.

1250 Kristiansen, S. and Farbrot, T., (1991). Nitrogen uptake rates in phytoplankton and ice algae in the Barents Sea. *Polar*  
1251 *research*, 10(1), pp.187-192.

1252 Kustka, A.B., Sañudo-Wilhelmy, S.A., Carpenter, E.J., Capone, D., Burns, J. and Sunda, W.G., (2003). Iron requirements  
1253 for dinitrogen-and ammonium-supported growth in cultures of *Trichodesmium* (IMS 101): Comparison with nitrogen  
1254 fixation rates and iron: Carbon ratios of field populations. *Limnology and Oceanography*, 48(5), pp.1869-1884.

1255 La Roche, J. (1983). Ammonium regeneration: its contribution to phytoplankton nitrogen requirements in a eutrophic  
1256 environment. *Marine Biology*, 75(2-3), pp.231-240.

1257 Landry, M.R., Selph, K.E., Brown, S.L., Abbott, M.R., Measures, C.I., Vink, S., Allen, C.B., Calbet, A., Christensen, S.  
1258 and Nolla, H., (2002). Seasonal dynamics of phytoplankton in the Antarctic Polar Front region at 170° W. *Deep Sea*  
1259 *Research Part II: Topical Studies in Oceanography*, 49(9-10), pp.1843-1865.

1260 Laubscher, R.K., Perissinotto, R. and McQuaid, C.D., (1993). Phytoplankton production and biomass at frontal zones in  
1261 the Atlantic sector of the Southern Ocean. *Polar biology*, 13(7), pp.471-481.

1262 Lauderdale, J.M., Garabato, A.C.N., Oliver, K.I., Follows, M.J. and Williams, R.G., (2013). Wind-driven changes in  
1263 Southern Ocean residual circulation, ocean carbon reservoirs and atmospheric CO<sub>2</sub>. *Climate dynamics*, 41(7-8), pp.2145-  
1264 2164.

1265 Lee, S.H., Joo, H.M., Liu, Z., Chen, J. and He, J., (2012). Phytoplankton productivity in newly opened waters of the  
1266 Western Arctic Ocean. *Deep Sea Research Part II: Topical Studies in Oceanography*, 81, pp.18-27.

1267 Lee, S.H., Yun, M.S., Kim, B.K., Joo, H., Kang, S.H., Kang, C.K. and Whitledge, T.E., (2013). Contribution of small  
1268 phytoplankton to total primary production in the Chukchi Sea. *Continental Shelf Research*, 68, pp.43-50.

1269 Legrand, M., Ducroz, F., Wagenbach, D., Mulvaney, R. and Hall, J., (1998). Ammonium in coastal Antarctic aerosol and  
1270 snow: Role of polar ocean and penguin emissions. *Journal of Geophysical Research: Atmospheres*, 103(D9), pp.11043-  
1271 11056.

1272 Lehette, P., Tovar-Sánchez, A., Duarte, C.M. and Hernández-León, S., (2012). Krill excretion and its effect on primary  
1273 production. *Marine Ecology Progress Series*, 459, pp.29-38.

1274 Le Moigne, F. A., Boye, M., Masson, A., Corvaisier, R., Grossteffan, E., Gueneugues, A., Pondaven, P., Le Moigne, F. A.  
1275 C., Boye, M., Corvaisier, R., Guéneugues, A., & Pondaven, P. (2013). Description of the biogeochemical features of the  
1276 subtropical southeastern Atlantic and the Southern Ocean south of South Africa during the austral summer of the  
1277 International Polar Year. *European Geosciences Union*, 10(10), pp.281-295.

1278 Lin, C. T., Jickells, T. D., Baker, A. R., Marca, A., & Johnson, M. T. (2016). Aerosol isotopic ammonium signatures over  
1279 the remote Atlantic Ocean. *Atmospheric Environment*, 133, pp.165-169.

1280 Lipschultz, F., (2008). Isotope tracer methods for studies of the marine nitrogen cycle. *Nitrogen in the Marine*  
1281 *Environment*, 2nd Edition, Academic Press: Burlington, MA, USA, pp.1345-1384.

1282 Llort, J., Lévy, M., Sallée, J.B., and Tagliabue, A., (2019). Nonmonotonic response of primary production and export to  
1283 changes in mixed-layer depth in the Southern Ocean. *Geophysical Research Letters*, 46(6), pp.3368-3377.

1284 Longhurst, A. R. (1998). Ecological Geography of the Sea. Academic Press, San Diego, CA.

1285 Lourey, M. J., Trull, T. W., and Sigman, D. M. (2003). Sensitivity of  $\delta^{15}\text{N}$  of nitrate, surface suspended and deep  
1286 sinking particulate nitrogen to seasonal nitrate depletion in the Southern Ocean. *Global Biogeochemical Cycles*, 17(3).

1287 Lu, S., Liu, X., Liu, C., Cheng, G., and Shen, H., (2020). Influence of photoinhibition on nitrification by ammonia-  
1288 oxidizing microorganisms in aquatic ecosystems. *Reviews in Environmental Science and Bio/Technology*, pp.1-12.

1289 Lutjeharms, J. R. E., and Valentine, H. R. (1984). Southern ocean thermal fronts south of Africa. *Deep Sea Research Part*  
1290 *A, Oceanographic Research Papers*, 31(12), 1461-1475.

1291 Macko, S.A., Estep, M.L.F., Engel, M.H., and Hare, P.E., (1986). Kinetic fractionation of stable nitrogen isotopes during  
1292 amino acid transamination. *Geochimica et Cosmochimica Acta*, 50(10), pp.2143-2146.

1293 Maldonado, M.T., Allen, A.E., Chong, J.S., Lin, K., Leus, D., Karpenko, N. and Harris, S.L., (2006). Copper-dependent  
1294 iron transport in coastal and oceanic diatoms. *Limnology and oceanography*, 51(4), pp.1729-1743.

1295 Marie, D., Partensky, F., Jacquet, S., and Vaulot, D., (1997). Enumeration and cell cycle analysis of natural populations of  
1296 marine picoplankton by flow cytometry using the nucleic acid stain SYBR Green I. *Appl. Environ. Microbiol.*, 63(1),  
1297 pp.186-193.

1298 Marie, D., Simon, N., and Vaulot, D., (2005). Phytoplankton cell counting by flow cytometry. *Algal culturing*  
1299 *techniques*, 1, pp.253-267.

- Martin, J.H., Fitzwater, S.E., and Gordon, R.M., (1990). Iron deficiency limits phytoplankton growth in Antarctic waters. *Global Biogeochemical Cycles*, 4(1), pp.5-12.
- Martínez-García, A., Sigman, D.M., Ren, H., Anderson, R.F., Straub, M., Hodell, D.A., Jaccard, S.L., Eglinton, T.I., & Haug, G.H., (2014). Iron fertilization of the Subantarctic Ocean during the last ice age. *Science*, 343(6177), pp.1347-1350.
- Mayzaud, P., Razouls, S., Errhif, A., Tirelli, V. and Labat, J.P., (2002). Feeding, respiration and egg production rates of copepods during austral spring in the Indian sector of the Antarctic Ocean: role of the zooplankton community in carbon transformation. *Deep Sea Research Part I: Oceanographic Research Papers*, 49(6), pp.1027-1048.
- McIlvin, M.R. and Altabet, M.A., (2005). Chemical conversion of nitrate and nitrite to nitrous oxide for nitrogen and oxygen isotopic analysis in freshwater and seawater. *Analytical Chemistry*, 77(17), pp.5589-5595.
- McIlvin, M.R., and Casciotti, K.L., (2011). Technical updates to the bacterial method for nitrate isotopic analyses. *Analytical Chemistry*, 83(5), pp.1850-1856.
- Mdutyana, M., Thomalla, S.J., Philibert, R., Ward, B.B., and Fawcett, S.E., (2020). The seasonal cycle of nitrogen uptake and nitrification in the Atlantic sector of the Southern Ocean. *Global Biogeochemical Cycles*, 34(7), p.e2019GB006363.
- Mdutyana, M., (2021). Mixed layer nitrogen cycling in the Southern Ocean: seasonality, kinetics, and biogeochemical implications. (PhD dissertation, University of Cape Town).
- Mei, Z.P., Finkel, Z.V., and Irwin, A.J., (2009). Light and nutrient availability affect the size-scaling of growth in phytoplankton. *Journal of theoretical biology*, 259(3), pp.582-588.
- Mengesha, S., Dehairs, F., Fiala, M., Elskens, M., and Goeyens, L. (1998). Seasonal variation of phytoplankton community structure and nitrogen uptake regime in the Indian Sector of the Southern Ocean. *Polar Biology*, 20(4), pp.259-272.
- Möbius, J., (2013). Isotope fractionation during nitrogen remineralization (ammonification): Implications for nitrogen isotope biogeochemistry. *Geochimica et Cosmochimica Acta*, 105, pp.422-432.
- Mongin, M., Nelson, D.M., Pondaven, P., & Tréguer, P., (2006). Simulation of upper-ocean biogeochemistry with a flexible-composition phytoplankton model: C, N and Si cycling and Fe limitation in the Southern Ocean. *Deep Sea Research Part II: Topical Studies in Oceanography*, 53(5-7), pp.601-619.
- Mongwe, N., Vichi, M. and Monteiro, P., (2018). The seasonal cycle of pCO<sub>2</sub> and CO<sub>2</sub> fluxes in the Southern Ocean: diagnosing anomalies in CMIP5 Earth system models. *Biogeosciences*, 15(9), pp.2851-2872.
- Moore, J.K. and Abbott, M.R., (2000). Phytoplankton chlorophyll distributions and primary production in the Southern Ocean. *Journal of Geophysical Research: Oceans*, 105(C12), pp.28709-28722.
- Mordy, C.W., Penny, D.M. and Sullivan, C.W., (1995). Spatial distribution of bacterioplankton biomass and production in the marginal ice-edge zone of the Weddell-Scotia Sea during austral winter. *Marine Ecology Progress Series*, 122, pp.9-19.
- Morel, F.M., Hudson, R.J., and Price, N.M., (1991). Limitation of productivity by trace metals in the sea. *Limnology and Oceanography*, 36(8), pp.1742-1755.
- Mtshali, T.N., van Horsten, N.R., Thomalla, S.J., Ryan-Keogh, T.J., Nicholson, S.A., Roychoudhury, A.N., Bucciarelli, E., Sarthou, G., Tagliabue, A. and Monteiro, P.M., (2019). Seasonal depletion of the dissolved iron reservoirs in the sub-Antarctic zone of the Southern Atlantic Ocean. *Geophysical Research Letters*, 46(8), pp.4386-4395.
- Munk, W.H., and Riley, G., (1952). Absorption of nutrients by aquatic plants. *Journal of Marine Research*, 11, pp. 215-240.
- Murphy, J., and Riley, J.P., (1962). A modified single solution method for the determination of phosphate in natural waters. *Analytica chimica acta*, 27, pp.31-36.
- Nelson, D.M., Brzezinski, M.A., Sigmon, D.E. and Franck, V.M., (2001). A seasonal progression of Si limitation in the Pacific sector of the Southern Ocean. *Deep Sea Research Part II: Topical Studies in Oceanography*, 48(19-20), pp.3973-3995.
- Nicholson, S.A., Lévy, M., Jouanno, J., Capet, X., Swart, S. and Monteiro, P.M., (2019). Iron supply pathways between the surface and subsurface waters of the Southern Ocean: from winter entrainment to summer storms. *Geophysical Research Letters*, 46(24), pp.14567-14575.
- Olson, R.J. (1981). Differential photoinhibition of marine nitrifying bacteria: a possible mechanism for the formation of the primary nitrite maximum.
- Orsi, A. H., Whitworth, T., and Nowlin, W. D. (1995). On the meridional extent and fronts of the Antarctic Circumpolar Current. *Deep-Sea Research Part I*, 42(5), pp.641-673.
- Owens, N.J.P., Priddle, J. and Whitehouse, M.J., (1991). Variations in phytoplanktonic nitrogen assimilation around South Georgia and in the Bransfield Strait (Southern Ocean). *Marine Chemistry*, 35(1-4), pp.287-304.
- Pachiadaki, M.G., Sintès, E., Bergauer, K., Brown, J.M., Record, N.R., Swan, B.K., Mathyer, M.E., Hallam, S.J., Lopez-Garcia, P., Takaki, Y. and Nunoura, T., (2017). Major role of nitrite-oxidizing bacteria in dark ocean carbon fixation. *Science*, 358(6366), pp.1046-1051.

Painter, S.C., Patey, M.D., Tarran, G.A. and Torres-Valdés, S., (2014). Picoeukaryote distribution in relation to nitrate uptake in the oceanic nitracline. *Aquatic Microbial Ecology*, 72(3), pp.195-213.

Palenik, B., Brahamsha, B., Larimer, F. W., Land, M., Hauser, L., Chain, P., Lamerdin, J., Regala, W., Allen, E. E., McCarren, J., Paulsen, I., Dufresne, A., Partensky, F., Webb, E. A., and Waterbury, J., (2003). The genome of a motile marine *Synechococcus*. *Nature*, 424(6952), 1037–1042.

Paulot, F., Jacob, D. J., Johnson, M. T., Bell, T. G., Baker, A. R., Keene, W. C., Lima, I. D., Doney, S. C., and Stock, C. A., (2015). Global oceanic emission of ammonia: Constraints from seawater and atmospheric observations. *Global Biogeochemical Cycles*, 29(8), pp.1165–1178.

Pausch, F., Bischof, K. and Trimborn, S., (2019). Iron and manganese co-limit growth of the Southern Ocean diatom *Chaetoceros debilis*. *Plos one*, 14(9), p.e0221959.

Pearce, I., Davidson, A. T., Thomson, P. G., Wright, S., and van den Enden, R. (2010). Marine microbial ecology off East Antarctica (30 - 80°E): Rates of bacterial and phytoplankton growth and grazing by heterotrophic protists. *Deep-Sea Research Part II: Topical Studies in Oceanography*, 57(9–10), 849–862.

Peng, X., Fuchsman, C.A., Jayakumar, A., Oleynik, S., Martens-Habbena, W., Devol, A.H. and Ward, B.B., (2015). Ammonia and nitrite oxidation in the Eastern Tropical North Pacific. *Global Biogeochemical Cycles*, 29(12), pp.2034-2049.

Philibert, R., Waldron, H. and Clark, D., (2015). A geographical and seasonal comparison of nitrogen uptake by phytoplankton in the Southern Ocean. *Ocean Science*, 11(2).

Plate, T., and Heiberger, R., (2019). abind: Combine multi-dimensional arrays. R package version 1.1. <https://cran.r-project.org/web/packages/abind>

Pomeroy, L. R., and Wiebe, W. J. (2001). Temperature and substrates as interactive limiting factors for marine heterotrophic bacteria. *Aquatic Microbial Ecology*, 23(2), pp.187–204.

Popp, B.N., Trull, T., Kenig, F., Wakeham, S.G., Rust, T.M., Tilbrook, B., Griffiths, B., Wright, S.W., Marchant, H.J., Bidigare, R.R., and Laws, E.A., (1999). Controls on the carbon isotopic composition of Southern Ocean phytoplankton. *Global Biogeochemical Cycles*, 13(4), pp.827-843.

Prézelin, B.B., Hofmann, E.E., Mengelt, C. and Klinck, J.M., (2000). The linkage between Upper Circumpolar Deep Water (UCDW) and phytoplankton assemblages on the west Antarctic Peninsula continental shelf. *Journal of Marine Research*, 58(2), pp.165-202.

Price, N.M., Ahner, B.A. and Morel, F.M., (1994). The equatorial Pacific Ocean: Grazer-controlled phytoplankton populations in an iron-limited ecosystem I. *Limnology and Oceanography*, 39(3), pp.520-534.

Priddle, J., Nedwell, D.B., Whitehouse, M.J., Reay, D.S., Savidge, G., Gilpin, L.C., Murphy, E.J. and Ellis-Evans, J.C., (1998). Re-examining the Antarctic Paradox: speculation on the Southern Ocean as a nutrient-limited system. *Annals of Glaciology*, 27, pp.661-668.

Primeau, F. W., Holzer, M., and DeVries, T. (2013). Southern Ocean nutrient trapping and the efficiency of the biological pump. *Journal of Geophysical Research: Oceans*, 118(5), pp.2547–2564.

R Core Team (2020). R: A language and environment for statistical computing. R Foundation for Statistical Computing, Vienna, Austria. URL <https://www.R-project.org/>.

Raven, J.A., (1988). The iron and molybdenum use efficiencies of plant growth with different energy, carbon and nitrogen sources. *New Phytologist*, 109(3), pp.279-287.

Reay, D. S., Priddle, J., Nedwell, D. B., Whitehouse, M. J., Ellis-Evans, J. C., Deubert, C., and Connelly, D. P. (2001). Regulation by low temperature of phytoplankton growth and nutrient uptake in the Southern Ocean. *Marine Ecology Progress Series*, 219(1990), pp.51–64.

Rees, A., Woodward, M. and Joint, I., (1999). Measurement of nitrate and ammonium uptake at ambient concentrations in oligotrophic waters of the North-East Atlantic Ocean. *Marine Ecology Progress Series*, 187, pp.295-300.

Rembauville, M., Briggs, N., Ardyna, M., Uitz, J., Catala, P., Penkerc'h, C., Poteau, A., Claustre, H., and Blain, S., (2017). Plankton assemblage estimated with BGC-Argo floats in the Southern Ocean: Implications for seasonal successions and particle export. *Journal of Geophysical Research: Oceans*, 122(10), pp.8278-8292.

Ren, H., Sigman, D.M., Thunell, R.C. and Prokopenko, M.G., (2012). Nitrogen isotopic composition of planktonic foraminifera from the modern ocean and recent sediments. *Limnology and Oceanography*, 57(4), pp.1011-1024.

Revilla, M., Alexander, J., and Gilbert, P.M., (2005). Urea analysis in coastal waters: comparison of enzymatic and direct methods. *Limnology and Oceanography: Methods*, 3(7), pp.290-299.

Richardson, T.L. and Jackson, G.A., (2007). Small phytoplankton and carbon export from the surface ocean. *Science*, 315(5813), pp.838-840.

Rintoul, S.R., and Trull, T.W., (2001). Seasonal evolution of the mixed layer in the Subantarctic Zone south of Australia. *Journal of Geophysical Research: Oceans*, 106(C12), pp.31447-31462.

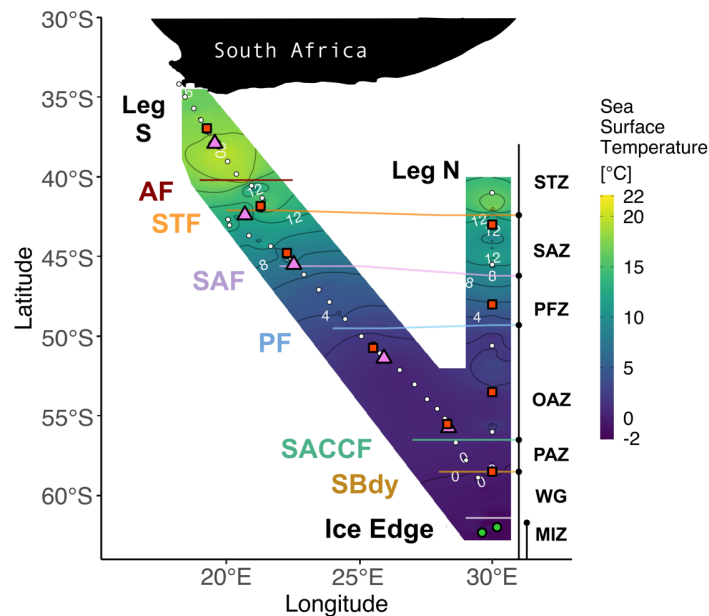
- Robinson, R.S., Jones, C.A., Kelly, R.P., Love, A., Closset, I., Rafter, P.A. and Brzezinski, M., (2020). A Test of the Diatom-Bound Paleoproxy: Tracing the Isotopic Composition of Nutrient-Nitrogen Into Southern Ocean Particles and Sediments. *Global Biogeochemical Cycles*, 34(10), p.e2019GB006508.
- Rodrigues, R.M., and Williams, P.J.L.B., (2001). Heterotrophic bacterial utilization of nitrogenous and nonnitrogenous substrates, determined from ammonia and oxygen fluxes. *Limnology and Oceanography*, 46(7), pp.1675-1683.
- Sallée, J.B., Speer, K.G. and Rintoul, S.R., (2010). Zonally asymmetric response of the Southern Ocean mixed-layer depth to the Southern Annular Mode. *Nature Geoscience*, 3(4), pp.273-279.
- Sambrotto, R.N. and Mace, B.J., (2000). Coupling of biological and physical regimes across the Antarctic Polar Front as reflected by nitrogen production and recycling. *Deep Sea Research Part II: Topical Studies in Oceanography*, 47(15-16), pp.3339-3367.
- Santoro, A.E., Sakamoto, C.M., Smith, J.M., Plant, J.N., Gehman, A.L., Worden, A.Z., Johnson, K.S., Francis, C.A. and Casciotti, K.L., (2013). Measurements of nitrite production in and around the primary nitrite maximum in the central California Current. *Biogeochemistry*, 10(11), pp.7395-7410.
- Sarmiento, J.L., and Orr, J.C., (1991). Three-dimensional simulations of the impact of Southern Ocean nutrient depletion on atmospheric CO<sub>2</sub> and ocean chemistry. *Limnology and Oceanography*, 36(8), pp.1928-1950.
- Sarmiento, J.L., and Toggweiler, J.R., (1984). A new model for the role of the oceans in determining atmospheric pCO<sub>2</sub>. *Nature*, 308(5960), pp.621-624.
- Sarmiento, J. L., Gruber, N., Brzezinski, M. A., and Dunne, J. P. (2004). High-latitude controls of thermocline nutrients and low latitude biological productivity. *Nature*, 427(6969), pp.56–60.
- Savoye, N., Dehairs, F., Elskens, M., Cardinal, D., Kopczyńska, E.E., Trull, T.W., Wright, S., Baeyens, W., and Griffiths, F.B., (2004). Regional variation of spring N-uptake and new production in the Southern Ocean. *Geophysical Research Letters*, 31(3).
- Schaafsma, F. L., Cherel, Y., Flores, H., van Franeker, J. A., Lea, M. A., Raymond, B., and van de Putte, A. P. (2018). Review: the energetic value of zooplankton and nekton species of the Southern Ocean. *Marine Biology*, 165(8), pp. 1–35.
- Scharek, R., Smetacek, V., Fährbach, E., Gordon, L.I., Rohardt, G., and Moore, S., (1994). The transition from winter to early spring in the eastern Weddell Sea, Antarctica: plankton biomass and composition in relation to hydrography and nutrients. *Deep Sea Research Part I: Oceanographic Research Papers*, 41(8), pp.1231-1250.
- Schön, G. H., and Engel, H. (1962). Der Einfluß des Lichtes auf *Nitrosomonas europaea* Win. *Archiv Für Mikrobiologie*, 42(4), pp.415-428.
- Sedwick, P. N., Bowie, A. R., and Trull, T. W. (2008). Dissolved iron in the Australian sector of the Southern Ocean (CLIVAR SR3 section): Meridional and seasonal trends. *Deep-Sea Research Part I: Oceanographic Research Papers*, 55(8), pp.911–925.
- Semeneh, M., Dehairs, F., Elskens, M., Baumann, M. E. M., Kopczynska, E. E., Lancelot, C., and Goeyens, L. (1998). Nitrogen uptake regime and phytoplankton community structure in the Atlantic and Indian sectors of the Southern Ocean. *Journal of Marine Systems*, 17(1-4), pp.159–177.
- Serebrennikova, Y. M., and Fanning, K. A. (2004). Nutrients in the Southern Ocean GLOBEC region: Variations, water circulation, and cycling. *Deep-Sea Research Part II: Topical Studies in Oceanography*, 51(17–19), pp.1981–2002.
- Shadwick, E.H., Trull, T.W., Tilbrook, B., Sutton, A.J., Schulz, E., and Sabine, C.L., (2015). Seasonality of biological and physical controls on surface ocean CO<sub>2</sub> from hourly observations at the Southern Ocean Time Series site south of Australia. *Global Biogeochemical Cycles*, 29(2), pp.223-238.
- Shafiee, R.T., Snow, J.T., Zhang, Q., and Rickaby, R.E., (2019). Iron requirements and uptake strategies of the globally abundant marine ammonia-oxidising archaeon, *Nitrosopumilus maritimus* SCM1. *The ISME journal*, 13(9), pp.2295-2305.
- Shiozaki, T., Fujiwara, A., Ijichi, M., Harada, N., Nishino, S., Nishi, S., Nagata, T. and Hamasaki, K., (2018). Diazotroph community structure and the role of nitrogen fixation in the nitrogen cycle in the Chukchi Sea (western Arctic Ocean). *Limnology and Oceanography*, 63(5), pp.2191-2205.
- Sigman, D. M., Altabet, M. A., McCorkle, D. C., Francois, R., and Fischer, G. (1999). The  $\delta^{15}\text{N}$  of nitrate in the southern ocean: Consumption of nitrate in surface waters. *Global Biogeochemical Cycles*, 13(4), pp.1149–1166.
- Sigman, D.M. and Boyle, E.A., (2000). Glacial/interglacial variations in atmospheric carbon dioxide. *Nature*, 407(6806), pp.859-869.
- Silfer, J.A., Engel, M.H. and Macko, S.A., (1992). Kinetic fractionation of stable carbon and nitrogen isotopes during peptide bond hydrolysis: experimental evidence and geochemical implications. *Chemical Geology: Isotope Geoscience section*, 101(3-4), pp.211-221.
- Sipler, R.E. and Bronk, D.A., (2015). Dynamics of dissolved organic nitrogen. *Biogeochemistry of marine dissolved organic matter*, pp.127-232.
- Smart, S. M., Fawcett, S. E., Thomalla, S. J., Weigand, M. A., Reason, C. J. C., and Sigman, D. M. (2015). Isotopic evidence for nitrification in the Antarctic winter mixed layer. *Global Biogeochemical Cycles*, 29(4), 427–445.

- Smart, S.M., Fawcett, S.E., Ren, H., Schiebel, R., Tompkins, E.M., Martínez-García, A., Stimmann, L., Roychoudhury, A., Haug, G.H. and Sigman, D.M., (2020). The Nitrogen Isotopic Composition of Tissue and Shell-Bound Organic Matter of Planktic Foraminifera in Southern Ocean Surface Waters. *Geochemistry, Geophysics, Geosystems*, 21(2), p.e2019GC008440.
- Smith, J. M., Chavez, F. P., and Francis, C. A. (2014). Ammonium Uptake by Phytoplankton Regulates Nitrification in the Sunlit Ocean. *PLoS ONE*, 9(9), e108173.
- Smith Jr, W.O. and Harrison, W.G., (1991). New production in polar regions: the role of environmental controls. *Deep Sea Research Part A: Oceanographic Research Papers*, 38(12), pp.1463-1479.
- Smith Jr, W.O. and Lancelot, C., (2004). Bottom-up versus top-down control in phytoplankton of the Southern Ocean. *Antarctic Science*, 16(4), p.531.
- Smith Jr, W.O., Marra, J., Hiscock, M.R. and Barber, R.T., (2000). The seasonal cycle of phytoplankton biomass and primary productivity in the Ross Sea, Antarctica. *Deep Sea Research Part II: Topical Studies in Oceanography*, 47(15-16), pp.3119-3140.
- Soares, M.A., Bhaskar, P.V., Naik, R.K., Dessai, D., George, J., Tiwari, M. and Anilkumar, N., (2015). Latitudinal  $\delta^{13}\text{C}$  and  $\delta^{15}\text{N}$  variations in particulate organic matter (POM) in surface waters from the Indian ocean sector of Southern Ocean and the Tropical Indian Ocean in 2012. *Deep Sea Research Part II: Topical Studies in Oceanography*, 118, pp.186-196.
- Sokolov, S. and Rintoul, S.R., (2007). On the relationship between fronts of the Antarctic Circumpolar Current and surface chlorophyll concentrations in the Southern Ocean. *Journal of Geophysical Research: Oceans*, 112(C7).
- Sosik, H.M. and Olson, R.J., (2002). Phytoplankton and iron limitation of photosynthetic efficiency in the Southern Ocean during late summer. *Deep Sea Research Part I: Oceanographic Research Papers*, 49(7), pp.1195-1216.
- Steinberg, D.K. and Saba, G.K., (2008). Nitrogen consumption and metabolism in marine zooplankton. In *Nitrogen in the marine environment* (pp. 1135-1196). Elsevier Inc.
- Strickland, J.D.H. and Parsons, T.R., (1972). A practical handbook of seawater analysis.
- Strzepek, R.F., Boyd, P.W. and Sunda, W.G., (2019). Photosynthetic adaptation to low iron, light, and temperature in Southern Ocean phytoplankton. *Proceedings of the National Academy of Sciences*, 116(10), pp.4388-4393.
- Studer, A.S., Sigman, D.M., Martínez-García, A., Benz, V., Winckler, G., Kuhn, G., Esper, O., Lamy, F., Jaccard, S.L., Wacker, L. and Oleynek, S., (2015). Antarctic Zone nutrient conditions during the last two glacial cycles. *Paleoceanography*, 30(7), pp.845-862.
- Sunda, W.G. and Huntsman, S.A., (1997). Interrelated influence of iron, light and cell size on marine phytoplankton growth. *Nature*, 390(6658), pp.389-392.
- Tagliabue, A., Mtsali, T., Aumont, O., Bowie, A.R., Klunder, M.B., Roychoudhury, A.N. and Swart, S., (2012). A global compilation of dissolved iron measurements: focus on distributions and processes in the Southern Ocean. *Biogeosciences*, 9(6), pp.2333-2349.
- Tagliabue, A., Sallée, J.B., Bowie, A.R., Lévy, M., Swart, S., and Boyd, P.W., (2014). Surface-water iron supplies in the Southern Ocean sustained by deep winter mixing. *Nature Geoscience*, 7(4), pp.314-320.
- Takao, S., Hirawake, T., Wright, S.W., and Suzuki, K., (2012). Variations of net primary productivity and phytoplankton community composition in the Indian sector of the Southern Ocean as estimated from ocean color remote sensing data. *Biogeosciences*, 9(10), pp.3875-3890.
- Talmy, D., Martiny, A.C., Hill, C., Hickman, A.E., and Follows, M.J., (2016). Microzooplankton regulation of surface ocean POC: PON ratios. *Global Biogeochemical Cycles*, 30(2), pp.311-332.
- Tevlin, A.G., and Murphy, J.G., (2019). Atmospheric Ammonia: Measurements, Modeling, and Chemistry–Climate Interactions. *Advances In Atmospheric Chemistry-Volume 2: Organic Oxidation And Multiphase Chemistry*, 2, p.1.
- Thomalla, S.J., Waldron, H.N., Lucas, M.I., Read, J.F., Anson, I.J., and Pakhomov, E., (2011). Phytoplankton distribution and nitrogen dynamics in the southwest indian subtropical gyre and Southern Ocean waters. *Ocean Science*, 7(1), pp.113-127.
- Tilzer, M.M., and Dubinsky, Z., (1987). Effects of temperature and day length on the mass balance of Antarctic phytoplankton. *Polar Biology*, 7(1), pp.35-42.
- Timmermans, K.R., Van Leeuwe, M.A., De Jong, J.T.M., McKay, R.M.L., Nolting, R.F., Witte, H.J., Van Ooyen, J., Swagerman, M.J.W., Kloosterhuis, H. and De Baar, H.J., (1998). Iron stress in the Pacific region of the Southern Ocean: evidence from enrichment bioassays. *Marine Ecology Progress Series*, 166, pp.27-41.
- Tolar, B.B., Ross, M.J., Wallsgrove, N.J., Liu, Q., Aluwihare, L.I., Popp, B.N., and Hollibaugh, J.T. (2016). Contribution of ammonia oxidation to chemoautotrophy in Antarctic coastal waters. *ISME Journal*, 10(11), pp.2605–2619.
- Tréguer, P. and Jacques, G., (1992). Review Dynamics of nutrients and phytoplankton, and fluxes of carbon, nitrogen and silicon in the Antarctic Ocean. In *Weddell Sea Ecology* (pp. 149-162). Springer, Berlin, Heidelberg.



- Treibergs, L.A., Fawcett, S.E., Lomas, M.W. and Sigman, D.M., (2014). Nitrogen isotopic response of prokaryotic and eukaryotic phytoplankton to nitrate availability in Sargasso Sea surface waters. *Limnology and Oceanography*, 59(3), pp.972-985.
- Trull, T.W., Davies, D. and Casciotti, K., (2008). Insights into nutrient assimilation and export in naturally iron-fertilized waters of the Southern Ocean from nitrogen, carbon and oxygen isotopes. *Deep Sea Research Part II: Topical Studies in Oceanography*, 55(5-7), pp.820-840.
- Tupas, L., & Koike, I. (1990). Amino acid and ammonium utilization by heterotrophic marine bacteria grown in enriched seawater. *Limnology and Oceanography*, 35(5), 1145–1155.
- Utermöhl, H., (1958). Zur vervollkommnung der quantitativen phytoplankton-methodik: mit 1 Tabelle und 15 abbildungen im Text und auf 1 Tafel. *Internationale Vereinigung für theoretische und angewandte Limnologie: Mitteilungen*, 9(1), pp.1-38.
- Vaulot, D., Courties, C. and Partensky, F., (1989). A simple method to preserve oceanic phytoplankton for flow cytometric analyses. *Cytometry: The Journal of the International Society for Analytical Cytology*, 10(5), pp.629-635.
- Venkataramana, V., Anilkumar, N., Naik, R.K., Mishra, R.K. and Sabu, P., (2019). Temperature and phytoplankton size class biomass drives the zooplankton food web dynamics in the Indian Ocean sector of the Southern Ocean. *Polar Biology*, 42(4), pp.823-829.
- Viljoen, J.J., Weir, I., Fietz, S., Cloete, R., Loock, J., Philibert, R. and Roychoudhury, A.N., (2019). Links between the phytoplankton community composition and trace metal distribution in summer surface waters of the Atlantic southern ocean. *Frontiers in Marine Science*, 6, p.295.
- Volk, T., and Hoffert, M.I., (1985). Ocean carbon pumps: Analysis of relative strengths and efficiencies in ocean-driven atmospheric CO<sub>2</sub> changes. *The carbon cycle and atmospheric CO<sub>2</sub>: natural variations Archean to present*, 32, pp.99-110.
- Wadley, M.R., Jickells, T.D., and Heywood, K.J., (2014). The role of iron sources and transport for Southern Ocean productivity. *Deep Sea Research Part I: Oceanographic Research Papers*, 87, pp.82-94.
- Wan, X.S., Sheng, H.X., Dai, M., Zhang, Y., Shi, D., Trull, T.W., Zhu, Y., Lomas, M.W. and Kao, S.J., (2018). Ambient nitrate switches the ammonium consumption pathway in the euphotic ocean. *Nature communications*, 9(1), pp.1-9.
- Ward, B. B. (1985). Light and substrate concentration relationships with marine ammonium assimilation and oxidation rates. *Marine Chemistry*, 16(4), pp.301–316.
- Ward, B.B., (2005). Temporal variability in nitrification rates and related biogeochemical factors in Monterey Bay, California, USA. *Marine Ecology Progress Series*, 292, pp.97-109.
- Weber, L.H. and El-Sayed, S.Z., (1987). Contributions of the net, nano-and picoplankton to the phytoplankton standing crop and primary productivity in the Southern Ocean. *Journal of Plankton Research*, 9(5), pp.973-994.
- Wei, T., and Simko, V., (2017). R package "corrplot": Visualization of a Correlation Matrix (Version 0.84). Available from <https://github.com/taiyun/corrplot>
- Weir, I., Fawcett, S., Smith, S., Walker, D., Bornman, T. and Fietz, S., (2020). Winter biogenic silica and diatom distributions in the Indian sector of the Southern Ocean. *Deep Sea Research Part I: Oceanographic Research Papers*, 166, p.103421.
- Welschmeyer, N.A., (1994). Fluorometric analysis of chlorophyll a in the presence of chlorophyll b and pheopigments. *Limnology and Oceanography*, 39(8), pp.1985-1992.
- Wickham H (2016). *ggplot2: Elegant Graphics for Data Analysis*. Springer-Verlag New York. ISBN 978-3-319-24277-4, <https://ggplot2.tidyverse.org>.
- Xu, G., Chen, L., Zhang, M., Zhang, Y., Wang, J. and Lin, Q., (2019). Year-round records of bulk aerosol composition over the Zhongshan Station, Coastal East Antarctica. *Air Quality, Atmosphere & Health*, 12(3), pp.271-288.
- Yool, A., Martin, A.P., Fernández, C., & Clark, D.R., (2007). The significance of nitrification for oceanic new production. *Nature*, 447(7147), pp.999-1002.
- Yu G. (2019). shadowtext: Shadow Text Grob and Layer. R package version 0.0.7. <https://CRAN.R-project.org/package=shadowtext>
- Zakem, E. J., Al-Haj, A., Church, M. J., Van Dijken, G. L., Dutkiewicz, S., Foster, S. Q., Fulweiler, R. W., Mills, M. M., and Follows, M. J. (2018). Ecological control of nitrite in the upper ocean. *Nature Communications*, 9(1), pp.1–13.
- Zhang, Y., Qin, W., Hou, L., Zakem, E.J., Wan, X., Zhao, Z., Liu, L., Hunt, K.A., Jiao, N., Kao, S.J. and Tang, K., (2020). Nitrifier adaptation to low energy flux controls inventory of reduced nitrogen in the dark ocean. *Proceedings of the National Academy of Sciences*, 117(9), pp.4823-4830.
- Zhou, J., Delille, B., Kaartokallio, H., Kattner, G., Kuosa, H., Tison, J.L., Autio, R., Dieckmann, G.S., Evers, K.U., Jørgensen, L. and Kennedy, H., (2014). Physical and bacterial controls on inorganic nutrients and dissolved organic carbon during a sea ice growth and decay experiment. *Marine Chemistry*, 166, pp.59-69.

1578 **Figure and Table Captions**



1579  
1580 *Figure 1: Winter 2017 cruise track overlaid on sea surface temperature (SST) measured by the hull-*  
1581 *mounted thermosalinograph. The underway (Leg S) and CTD (Leg N) stations are indicated by white*  
1582 *circles. Stations at which net primary production (NPP), nitrogen uptake, and ammonium oxidation*  
1583 *experiments were conducted are denoted by red squares. The pink triangles indicate stations where only*  
1584 *NPP experiments were conducted while the green circles show stations where only ammonium oxidation*  
1585 *was measured. Solid lines indicate the positions of the fronts, identified from measurements of*  
1586 *temperature and salinity. Abbreviations for fronts: AF – Agulhas Front (~40.2°S); STF – Subtropical*  
1587 *Front (~42.1°S); SAF – Subantarctic Front (~45.6°S); PF – Polar Front (~49.5°S); SACCF – Southern*  
1588 *Antarctic Circumpolar Current Front (~56.5°S); SBDY – Southern Boundary (~58.5°S). Abbreviations*  
1589 *for zones: STZ – Subtropical Zone; SAZ – Subantarctic Zone; PFZ – Polar Frontal Zone; OAZ – Open*  
1590 *Antarctic Zone; PAZ – Polar Antarctic Zone; WG – Weddell Gyre; MIZ – Marginal Ice Zone. Together,*  
1591 *the OAZ and PAZ constitute the Antarctic Zone (AZ). See Text S1 for detailed definitions of the fronts*  
1592 *and zones. Figure produced using the package ggplot2 (Wickham, 2016).*

1593 *Table 1: Mean (± 1 SD) of surface ocean POC, PON, chl-a, and nutrient concentrations, cell abundances,*  
1594 *and nutrient uptake rates measured in each zone of the Southern Ocean in winter 2017. Where no SD is*  
1595 *given, only one sample was measured. The >0.3 µm and >2.7 µm size fractions are referred to as “bulk”*  
1596 *and “nano+”, respectively. “% of nano+” refers to the average relative contribution of the nano+ size*  
1597 *fraction to total chl-a, POC, or PON, calculated for each station within a zone. The f-ratio including pUrea*

1598 is only shown for zones where pUrea was measured at all stations. “ND” indicates no data available.  
 1599 Abbreviations as in Figure 1.

	STZ	SAZ	PFZ	OAZ	PAZ
NH <sub>4</sub> <sup>+</sup> (μM)	0.08±0.03	0.06±0.01	0.42±0.01	0.52±0.01	0.58±0.01
PO <sub>4</sub> <sup>3-</sup> (μM)	0.44±0.07	0.90±0.06	1.59±0.1	2.00±0.13	1.99±0.09
NO <sub>3</sub> <sup>-</sup> (μM)	3.6±0.2	10.5±0.5	21.5±0.2	26.7±0.4	27.5±0.4
Si(OH) <sub>4</sub> (μM)	2.6±0.1	2.5±1.8	6.6±0.1	40.3±0.5	45.0±0.8
NO <sub>2</sub> <sup>-</sup> (μM)	0.15±0.02	0.13±0.02	0.17±0.02	0.19±0.01	0.21±0.02
Urea (μM)	0.23±0.04	0.11±0.04	0.26±0.08	0.24	0.21±0.03
chl-a (bulk) (μg L <sup>-1</sup> )	0.65±0.08	0.43±0.05	0.35±0.03	0.25±0.02	0.21±0.00
chl-a (nano+) (μg L <sup>-1</sup> )	0.50±0.05	0.30±0.04	0.24±0.02	0.18±0.02	0.17±0.02
chl-a (pico) (μg L <sup>-1</sup> )	0.15±0.1	0.13±0.07	0.11±0.04	0.06±0.03	0.04±0.02
chl-a (% of nano+)	77.5±13.9	73.1±10.9	69.8±8.7	76.7±11.3	80.1±8.5
POC (bulk) (μM)	4.4±6.7	3.4±0.4	3.2±0.3	3.4±0.5	3.5±0.2
POC (nano+) (μM)	2.6±0.5	2.6±0.4	1.9±1.2	1.9±0.4	4.6
PON (bulk) (μM)	0.6±0.2	0.5±0.1	0.4±0.1	0.5±0.1	0.5±0.1
PON (nano+) (μM)	0.3±0.1	0.3±0.1	0.2±0.3	0.2±0.1	0.4±0.0
POC (% of nano+)	79.7±24.6	79.6±19.0	50.9±33.2	77.2±21.8	ND
PON (% of nano+)	69.0±31.9	67.1±17.2	53.8±24.1	67.0±21.9	51.1±24.7
POC:chl-a (g g <sup>-1</sup> )	103.0±22.1	102.5±14.4	122.5±11	234.1±29.2	219.3±1.0
POC:PON (M/M)	7.81±6.49	6.90±1.25	7.13±0.71	6.72±1.62	5.80±3.75
δ <sup>15</sup> N-PON	1.4±0.9	1.2±1.0	0.3±0.5	-1.3±0.5	-1.3±0.4
NPP (bulk) (nM day <sup>-1</sup> )	497.1±42.4	277.5±21.3	289.7±19.2	85.3±26.1	27.7±0.2
NPP (nano+) (nM day <sup>-1</sup> )	384.7±29.7	178.2±23.4	193.5	49.6±5.0	ND
pNH <sub>4</sub> <sup>+</sup> (bulk) (nM day <sup>-1</sup> )	5.7±0.8	8.9±1.1	12.9±0.4	4.8±0.1	3.0±0.8
pNH <sub>4</sub> <sup>+</sup> (nano+) (nM day <sup>-1</sup> )	4.0±1.1	4.1±1.2	4.2±4.7	3.1±0.4	ND
pNO <sub>3</sub> <sup>-</sup> (bulk) (nM day <sup>-1</sup> )	4.1±0.4	11.5±1.4	5.9±1	3.6±0.4	3.7±1.8
pNO <sub>3</sub> <sup>-</sup> (nano+) (nM day <sup>-1</sup> )	3.4±0.3	6.6±0.4	4.3±0.4	2.6±0.8	2.7±1.2
pUrea (bulk) (nM day <sup>-1</sup> )	7.5±0.6	6.9±0.3	6.5±1.0	2.1±0.3	0.6±0.01
pUrea (nano+) (nM day <sup>-1</sup> )	4.9±0.3	3.8±0.2	4.0±0.6	1.3±0.2	0.7±0.4
f-ratio (bulk) (including pUrea)	0.21±0.31	0.43±0.11	0.23±0.18	ND	0.51±0.53
f-ratio (bulk) (excluding pUrea)	0.43±0.32	0.57±0.12	0.31±0.18	0.43±0.16	0.55±0.54
NH <sub>4</sub> <sup>+</sup> ox (nM day <sup>-1</sup> )	9.3±0.5	12.9±0.6	11.1	17.7±0.6	14.3±1.0
Total microplankton (cells mL <sup>-1</sup> )	13±11	5±3	9±3	6±6	4±2
Centric diatoms (cells mL <sup>-1</sup> )	<1	<1	<1	<1	1±2
Pennate diatoms (cells mL <sup>-1</sup> )	2±4	<1	2±1	2±3	<1
Dinoflagellates (cells mL <sup>-1</sup> )	7±6	4±0	6±2	3±2	2±0
Micro-zooplankton (cells mL <sup>-1</sup> )	4±3	<1	2±2	1±2	<1
Nano-eukaryotes (cells mL <sup>-1</sup> )	ND	2.2±1.4 E+03	1.5±0.7 E+03	1.6±0.7 E+03	1.4E+03
Pico-eukaryotes (cells mL <sup>-1</sup> )	ND	4.5±2.9 E+03	4.9±3.7 E+03	1.5±0.5 E+03	8E+02
<i>Synechococcus</i> (cells mL <sup>-1</sup> )	ND	3.8±1.8 E+03	2.3±1.1 E+03	1.4±0.2 E+03	1E+03

1600  
1601

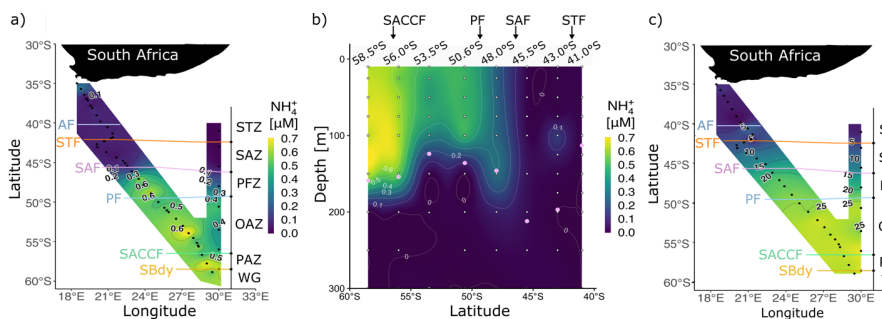


Figure 2: Concentrations of dissolved ammonium ( $\text{NH}_4^+$ ) a) at the surface for Legs S and N and b) with depth (0-300 m) for Leg N, and c) concentrations of nitrate ( $\text{NO}_3^-$ ) at the surface for Legs S and N. Pink circles in panel b show the mixed layer depth at the CTD stations. Abbreviations are as in Figure 1. Figure produced using the package ggplot2 (Wickham, 2016).

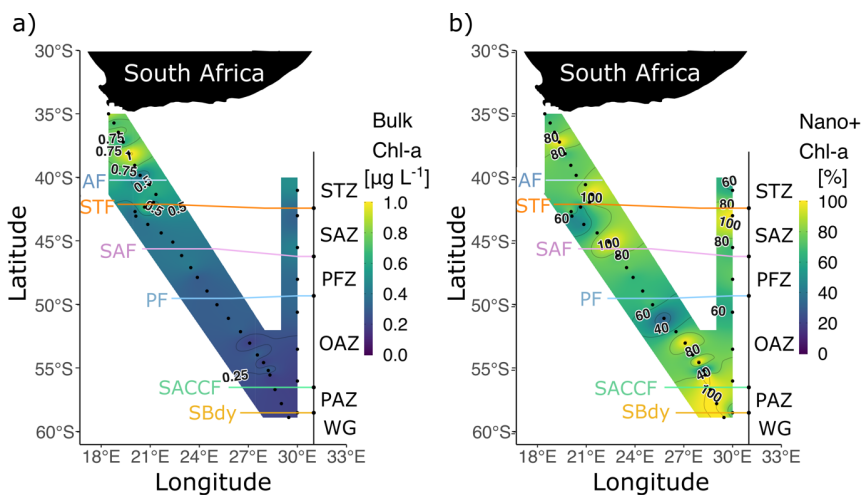
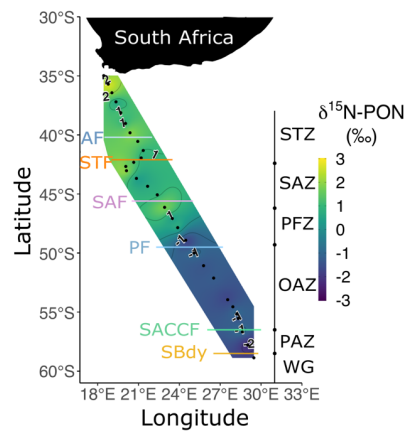


Figure 3: a) Bulk chlorophyll-a (chl-a) concentrations and b) the proportion of chlorophyll-a in the nano+ size fraction at the surface for Legs S and N. Abbreviations are as in Figure 1. Figure produced using the package ggplot2 (Wickham, 2016).



1611

1612 *Figure 4: Bulk  $\delta^{15}\text{N-PON}$  at the surface for Leg S in winter 2017. Two stations nearest South Africa at*  
 1613 *which biomass concentrations were extremely high have been excluded. Abbreviations are as in Figure*  
 1614 *1. Figure produced using the package ggplot2 (Wickham, 2016).*

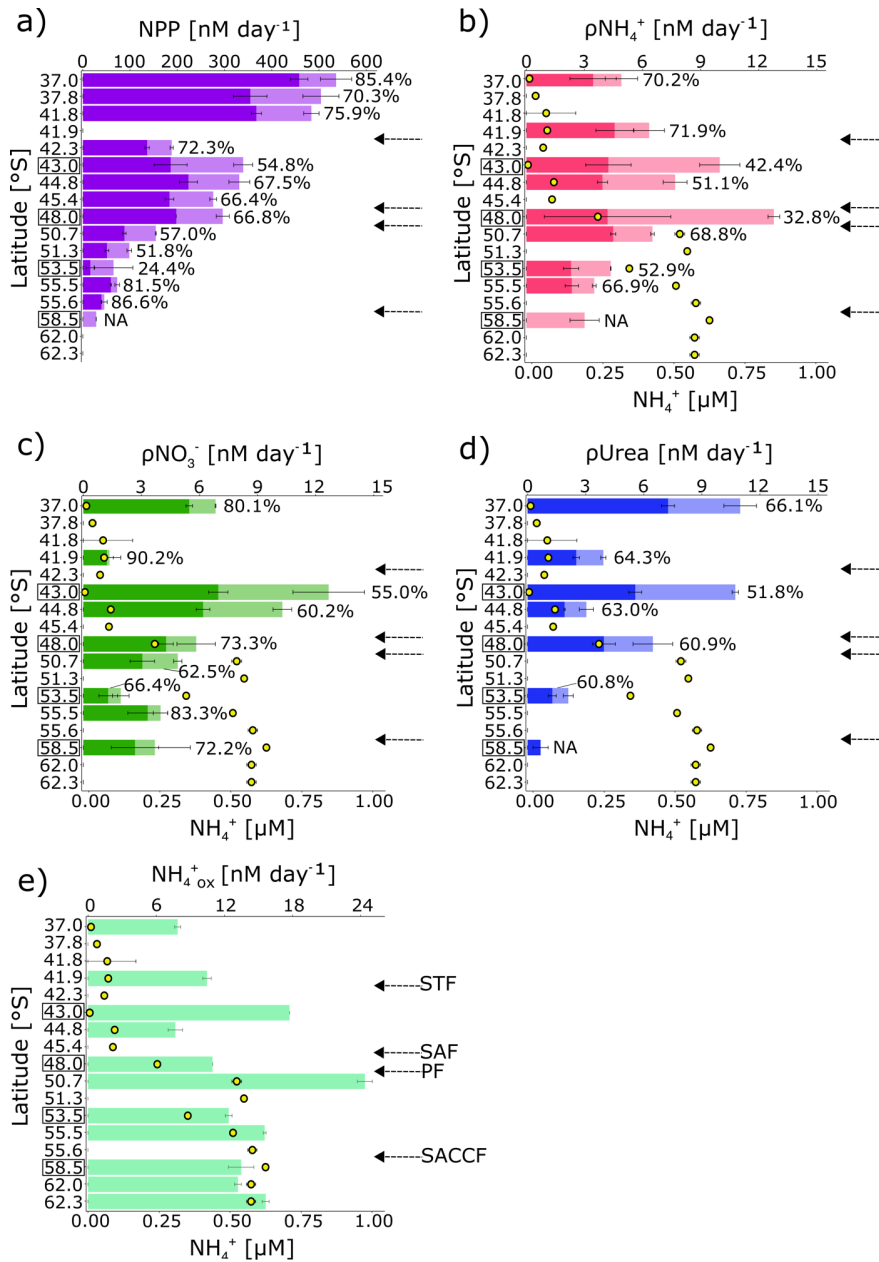
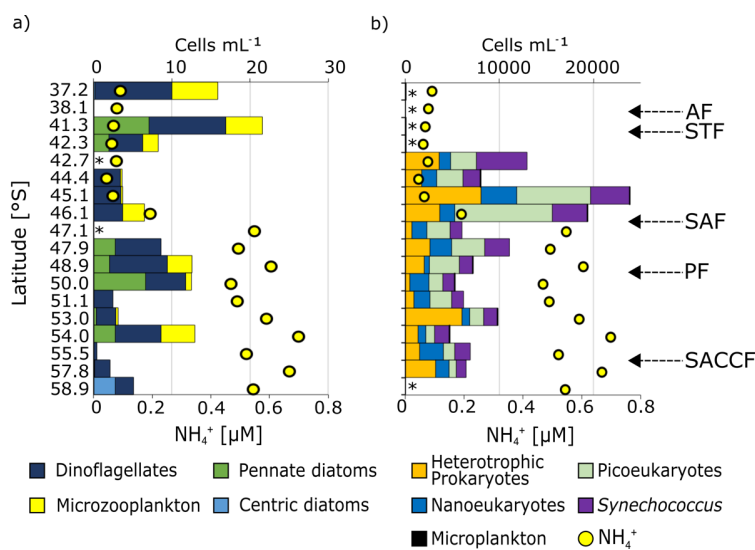


Figure 5: Surface rates of a) net primary production (NPP) and rates of b) ammonium (pNH<sub>4</sub><sup>+</sup>), c) nitrate (pNO<sub>3</sub><sup>-</sup>), and d) urea (pUrea) uptake by the pico (light colours) and nano+ (dark colours) size fractions, with the full length of the bars indicating the bulk rates, and e) NH<sub>4</sub><sup>+</sup> oxidation. Error bars indicate ±1

standard deviation of duplicate experiments. The percentage of total NPP and N uptake attributable to the nano+ size fraction is written next to each bar in panels a-d. NPP and  $\text{NH}_4^+$  uptake were not measured for the nano+ size fraction at 58.5°S, and urea uptake was not measured at 50.7°S and 55.5°S. Rates were not measured at the latitudes where no data are shown. In panels b-e, the surface  $\text{NH}_4^+$  concentration at each station is shown by the yellow circles. Leg N stations (at which samples were collected from Niskin bottles fired at 10 m) are indicated by black boxes surrounding the latitude. By contrast, samples were collected at the Leg S stations (no square surrounding the latitude) from the ship's underway system (~7 m). Fronts are indicated with arrows (labeled in panel e), and abbreviations are as in Figure 1. Figure produced using the package ggplot2 (Wickham, 2016).



**Figure 6:** Surface community composition for a) plankton  $\geq 15 \mu\text{m}$  (enumerated by microscopy) and b) the total community  $< 15 \mu\text{m}$  (enumerated by flow cytometry). For context, the surface  $\text{NH}_4^+$  concentration at each station is shown by the yellow circles. \* indicates stations at which no measurements were made while the absence of a bar with no \* indicates that no cells were detected. Note that the abundances shown on panel b (top x-axis) are  $> 2$  orders of magnitude greater than those shown in panel a. The “microplankton” shown in panel a are included on panel b (slim black bars) to illustrate the difference in abundance between the micro- and pico+nano populations. The frontal positions are indicated on panel b, with abbreviations as in Figure 1.

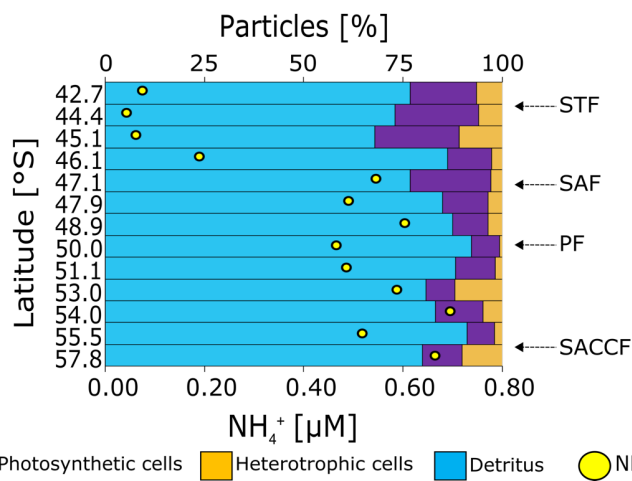
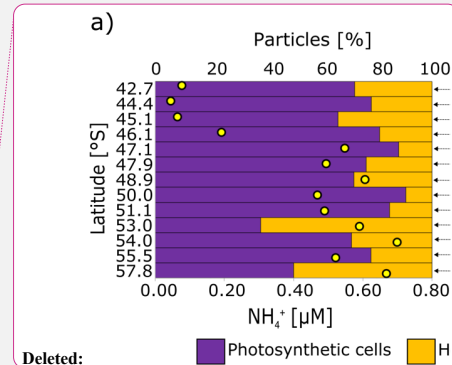


Figure 7: Relative contributions of photosynthetic, heterotrophic bacterial, and detrital particles to the total flow cytometry counts at the surface during leg S. The coincident  $\text{NH}_4^+$  concentrations are shown as yellow dots. Abbreviations are as in Figure 1.



**Deleted:** Relative abundances of a) total photosynthetic versus heterotrophic bacteria and b) detritus versus heterotrophic bacteria at the surface for Leg S. The surface  $\text{NH}_4^+$  concentration at each station is indicated by the yellow dots. The values in maroon text on the right side of panel a are the photosynthetic-to-heterotrophic cell ratios. The upper x-axis in panel b begins at 75% in order to highlight the (much smaller) heterotrophic bacterial contribution to the summed detrital + heterotrophic particles. Frontal abbreviations are as in Figure 1.



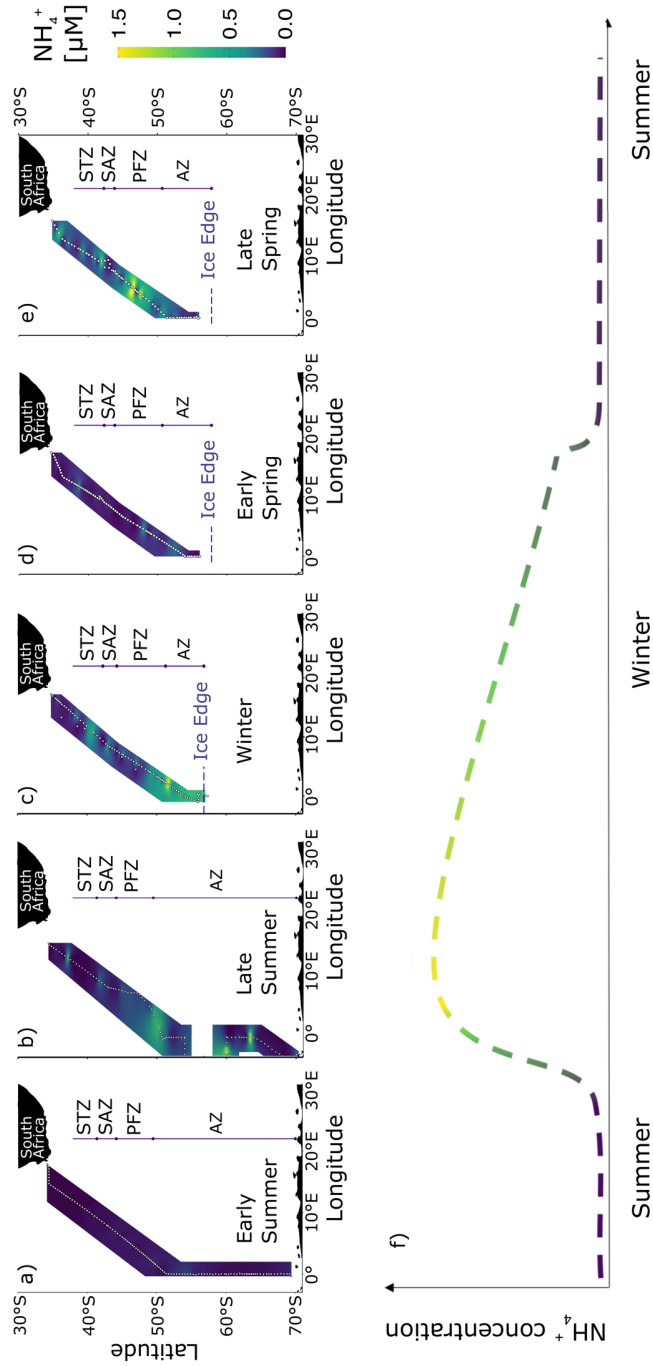
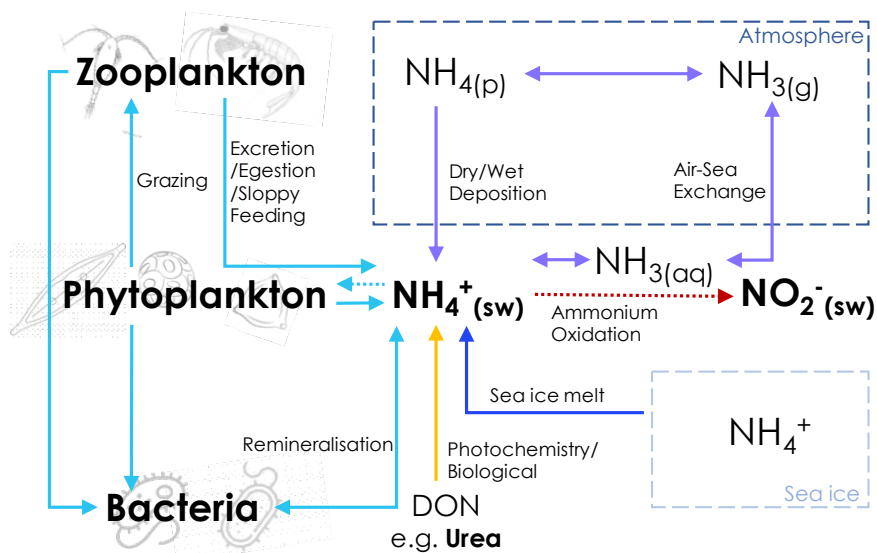


Figure 8: Surface concentrations of  $\text{NH}_4^+$  across the eastern Atlantic sector of the Southern Ocean measured between December 2018 and November 2019. Five unique transects (additional to the winter 2017 dataset presented in Fig. 2a) are shown: a) early summer 2018, b) late summer 2018, c) winter 2019, d) early spring 2019, and e) late spring 2019. f) The proposed seasonal cycle of  $\text{NH}_4^+$  concentrations in the mixed layer south of the Subantarctic Front. The colour gradient in panel f shows the transition between late summer and late winter. Panels a and b cover a latitudinal extent of 30–70°S, while panels c–e cover 30–60°S due to the presence of sea-ice. Abbreviations are as in Figure 1, with AZ referring to the combined OAZ and PAZ. Figure produced using the package ggplot2 (Wickham, 2016).



1653

1654 *Figure 9:* Schematic of the possible mixed-layer  $\text{NH}_4^+$  assimilation and production pathways. Bold text  
 1655 indicates components of the  $\text{NH}_4^+$  cycle that were directly measured in this study (seawater concentrations  
 1656 of  $\text{NH}_4^+$ ,  $\text{NO}_2^-$ , and urea; phytoplankton, bacterial, and microzooplankton cell abundances), and dotted  
 1657 lines indicate processes for which we have direct rate measurements (phytoplankton uptake of  $\text{NH}_4^+$ ;  
 1658 oxidation of  $\text{NH}_4^+$  to  $\text{NO}_2^-$ ). Dashed-line boxes represent the atmosphere and sea-ice, with all other  
 1659 processes occurring in the ocean. DON – dissolved organic nitrogen;  $\text{NH}_3(\text{aq})$  – aqueous (seawater)  
 1660 ammonia;  $\text{NH}_4(\text{p})$  – ammonium aerosols (including ammonium sulphate, ammonium bisulphate, and  
 1661 ammonium nitrate);  $\text{NH}_3(\text{g})$  – ammonia gas.